2816–2834 *Nucleic Acids Research, 2021, Vol. 49, No. 5* *Published online 22 February 2021*
doi: 10.1093/nar/gkab104

The human tRNA taurine modification enzyme GTPBP3 is an active GTPase linked to mitochondrial diseases

Gui-Xin Peng[1,2], Yong Zhang[1], Qin-Qin Wang[2], Qing-Run Li[3], Hong Xu[4], En-Duo Wang[1,2,*] and Xiao-Long Zhou[1,*]

[1]State Key Laboratory of Molecular Biology, CAS Center for Excellence in Molecular Cell Science, Shanghai Institute of Biochemistry and Cell Biology, Chinese Academy of Sciences, University of Chinese Academy of Sciences, 320 Yue Yang Road, Shanghai 200031, China, [2]School of Life Science and Technology, ShanghaiTech University, 393 Middle Hua Xia Road, Shanghai 201210, China, [3]CAS Key Laboratory of Systems Biology, CAS Center for Excellence in Molecular Cell Sciences, Shanghai Institute of Biochemistry and Cell Biology, Chinese Academy of Sciences, 320 Yue Yang Road, Shanghai 200031, China and [4]Shanghai Key Laboratory of Embryo Original Diseases, Shanghai Municipal Key Clinical Specialty, the International Peace Maternity and Child Health Hospital, School of Medicine, Shanghai Jiao Tong University, 910 Heng Shan Road, Shanghai 200030, China

Received October 20, 2020; Revised February 03, 2021; Editorial Decision February 05, 2021; Accepted February 09, 2021

ABSTRACT

GTPBP3 and MTO1 cooperatively catalyze 5-taurinomethyluridine (τm^5U) biosynthesis at the 34th wobble position of mitochondrial tRNAs. Mutations in tRNAs, GTPBP3 or MTO1, causing τm^5U hypomodification, lead to various diseases. However, efficient *in vitro* reconstitution and mechanistic study of τm^5U modification have been challenging, in part due to the lack of pure and active enzymes. A previous study reported that purified human GTPBP3 (hGTPBP3) is inactive in GTP hydrolysis. Here, we identified the mature form of hGTPBP3 and showed that hGTPBP3 is an active GTPase *in vitro* that is critical for tRNA modification *in vivo*. Unexpectedly, the isolated G domain and a mutant with the N-terminal domain truncated catalyzed GTP hydrolysis to only a limited extent, exhibiting high K_m values compared with that of the mature enzyme. We further described several important pathogenic mutations of hGTPBP3, associated with alterations in hGTPBP3 localization, structure and/or function *in vitro* and *in vivo*. Moreover, we discovered a novel cytoplasm-localized isoform of hGTPBP3, indicating an unknown potential non-canonical function of hGTPBP3. Together, our findings established, for the first time, the GTP hydrolysis mechanism of hGTPBP3 and laid a solid foundation for clarifying the τm^5U modification mechanism and etiology of τm^5U deficiency-related diseases.

INTRODUCTION

Mitochondria generate most of their cellular energy via oxidative phosphorylation (OXPHOS) and control various pivotal cellular functions (1,2). One particular feature of mitochondria in eukaryotes is that they harbor their own genome. Mammalian mitochondrial DNA (mtDNA) contains 37 genes, including genes of 2 rRNAs (12S and 16S) and 22 tRNAs, which are the minimal set of tRNAs for a decoding system, to decode 11 mtDNA-encoded mRNAs, the products (13 proteins) of which are essential for the assembly and function of respiratory chain complexes (3). Accordingly, mitochondrial protein synthesis is one of the most important processes and is of great significance for mitochondrial homeostasis and cellular functions. Notably, all the RNA components (4,5) of the mitochondrial translation system are encoded by mtDNA, while all the protein components, including aminoacyl-tRNA synthetases (6–9) and tRNA modification enzymes (10,11), are encoded by the nuclear genome.

Mitochondrial tRNA must undergo extensive posttranscriptional maturation, and one of the key processes is chemical nucleotide modification. Fifteen types of modifications at 118 positions in bovine mitochondrial tRNAs and 18 kinds of modifications at 137 positions in 22 human tRNAs have been identified (12,13). Most tRNA modifications occur at the anticodon loop, especially at the wobble position 34, which plays a crucial role in regulating the precision and efficiency of codon-anticodon interactions and expanding the decoding capability of a tRNA (10,14,15).

*To whom correspondence should be addressed. Tel: +86 21 54921247; Fax: +86 21 54921011; Email: xlzhou@sibcb.ac.cn
Correspondence may also be addressed to En-Duo Wang. Email: edwang@sibcb.ac.cn

The taurine modification (τm^5s^2U and τm^5U) (Supplementary Figure S1), present at wobble position U34 of the anticodon of five human mitochondrial tRNAs (τm^5U in hmtRNA^{Leu} (UUR), hmtRNA^{Trp}; τm^5s^2U in hmtRNA^{Lys}, hmtRNA^{Gln} and hmtRNA^{Glu}), is one of the few modification types that exists in only mitochondrial tRNAs, not cytosolic tRNAs (12). In fact, τm^5U is structurally similar to 5-carboxymethylaminomethyluridine ($cmnm^5U$) and occurs in tRNA^{Lys} (UUU), tRNA^{Glu} (UUC), tRNA^{Gln} (UUG), tRNA^{Leu} (UAA), tRNA^{Arg} (UCU) and tRNA^{Gly} (UCC) in bacteria and in mitochondrial tRNA^{Lys}, tRNA^{Glu}, and tRNA^{Gln} in yeast, which are jointly catalyzed by MnmE and MnmG or MSS1 and MTO1, respectively (16–18). In humans, GTP binding protein 3 (GTPBP3, MnmE/MSS1 homolog) and mitochondrial tRNA translation optimization 1 (MTO1, bacterial MnmG homolog) are two highly conserved tRNA-modifying enzymes involved in the formation of τm^5U (19). MTU1 catalyzes the 2-thiol group of τm^5U, generating τm^5s^2U, which seems to occur independent of taurine modification (19,20). *In vitro* $cmnm^5U$ modification activity has been successfully reconstituted with MnmE and MnmG, which form an $\alpha 2\beta 2$ heterotetrameric complex that uses glycine, methylene-THF (tetrahydrofolate), FAD (flavin adenine dinucleotide), NADH (nicotinamide adenine dinucleotide) and other cofactors as substrates (16,17). However, efficient τm^5U modification activity has never been realized *in vitro*, although overexpressed GTPBP3/MTO1 complexes precipitated from human cells are able to utilize similar substrates, using taurine in place of glycine, to produce limited amounts of τm^5U *in vitro* with the efficiency of 3.3% (19). It has been shown that τm^5s^2U and τm^5U modifications promote accurate decoding of NNR codons (N = U, C, A or G; R = A or G) and prevents misreading of NNY codons (Y = U or C) (4). For instance, τm^5U modification plays a pivotal role in efficient decoding of the UUG codon by stabilizing U:G wobble pairing at the ribosomal A site during the decoding process in translation (21,22).

Due to the critical role of τm^5U modification in mitochondrial mRNA decoding, it is not unexpected that defective τm^5U formation, due to either mtDNA-encoded tRNA mutation or nuclear genome-encoded tRNA modification enzyme mutations, would lead to mitochondrial malfunction and human disorders (21,23,24). For instance, the A3243G mutation in hmtRNA^{Leu} (UUR) leads to τm^5U modification defects, severely reduced UUG codon translation efficiency, and complex I and complex IV deficiency, thus causing MELAS (mitochondrial encephalomyopathy, lactic acidosis, and stroke-like episodes) (21,25). In parallel, the A8344G mutation in hmtRNA^{Lys} similarly leads to $\tau m^5(s^2)U$ formation deficiency and impairment in AAA and AAG codon decoding and thus causes MERRF (myoclonic epilepsy with ragged red fibers) (23,25). Notably, the hmtRNA^{Leu} (UUR) A3243G and hmtRNA^{Lys} A8344G mutations are the first described disease-causing genetic mutations in the mRNA translation pathway (26,27). However, the molecular basis for $\tau m^5(s^2)U$ modification defects induced by both A8344G and A3243G mutations has remained unclear for more than two decades. On the other hand, the deficient τm^5U modification caused by mutations in the genes encoding MTO1 and GTPBP3 was responsible for mitochondrial dysfunction (24,28,29). Mutations in MTO1 are associated with infantile hypertrophic cardiomyopathy, lactic acidosis, cognitive disability and seizures (24,30,31), while GTPBP3 mutations are implicated in hypertrophic cardiomyopathy, lactic acidosis, and encephalopathy (28). In human cell lines, depletion of *GTPBP3* results in deficient τm^5U modification, reduced efficiency of mitochondrial translation and deficiency of OXPHOS (19). Furthermore, *gtpbp3* knockdown and knockout zebrafish displayed a marked decrease in mitochondrial ATP generation, instability of OXPHOS, impairment of mitochondrial translation and defective development (32).

As one of the two enzymes involved in τm^5U modification, human GTPBP3 (hGTPBP3) itself, based on primary sequence alignment and crystal structures of its homologs (such as *Thermotoga maritima* MnmE (*Tm*MnmE) (PDB: 1XZP) and *Escherichia coli* MnmE (*Ec*MnmE) (PDB: 2GJ8)), has an N-terminal domain, a GTPase domain (G domain) and a helical domain (33–35). The G domain comprises the typical G1, G2, G3, and G4 motifs involved in the binding and hydrolysis of GTP (36). GTP hydrolysis has been shown to be essential for $cmnm^5U$ formation in bacteria (16,17). However, a previous study showed that hGTPBP3 could not be expressed in *E. coli*; both the full-length GTPBP3 fused with an N-terminal GST tag (GST-GTPBP3 precursor) and the isolated G domain are nearly inactive GTPases, eliciting a potentially unknown mechanism of human τm^5U modification. The inability to obtain active hGTPBP3 also suggests the low possibility or great difficulty of reconstituting human τm^5U modification *in vitro* (37). Despite the above evidence pinpointing the critical importance of τm^5U modification in mitochondrial translation, homeostasis, and organismal fitness and health, due to a lack of active enzymes and efficient *in vitro* τm^5U modification activity, the detailed basic molecular mechanism of τm^5U formation was hitherto unexplored. Furthermore, little is known about the detailed molecular mechanisms (defects in tRNA/enzyme structure, function, interaction etc.) underlying the pathogenesis linked with either tRNA or enzyme mutations.

To understand the biochemical mechanism of τm^5U modification of human mitochondrial tRNA, it is necessary to obtain either enzyme with high purity and activity. In the present work, we identified the mature form of hGTPBP3 and showed, for the first time, that hGTPBP3 possesses high intrinsic GTPase activity. However, the isolated G domain and an N-terminal domain truncated hGTPBP3 (ΔN-hGTPBP3) exhibited a very low GTPase catalytic efficiency and a high K_m value compared with the mature enzyme. Based on our established GTPase activity determination system, we further investigated the effect of a series of pathogenic hGTPBP3 mutations on mitochondrial targeting, protein stability and GTPase activity. We identified several key intramolecular interactions for GTPase *in vitro* and tRNA modification activity *in vivo*. Last, we identified a novel splicing variant of hGTPBP3 mRNA, which was expressed and exclusively distributed in the cytoplasm, imply-

ing an unexplored noncanonical function of the hGTPBP3 gene. In conclusion, we purified active hGTPBP3 and systematically investigated its GTPase *in vitro* and tRNA modification activity *in vivo*. Our results lay a solid foundation for *in vitro* activity reconstitution of τm^5U modification and for elucidation of the underlying mechanism in the future.

MATERIALS AND METHODS

Materials

Dithiothreitol (DTT), nucleoside triphosphates (NTPs), Tris–HCl, $MgCl_2$, NaCl, KCl, β-mercaptoethanol (β-ME), phenyl methylsulfonyl fluoride (PMSF), isopropyl β-D-1-thiogalactopyranoside (IPTG), and ethylene diamine tetraacetic acid (EDTA) were purchased from Sangon (Shanghai, China). The KOD-Plus Mutagenesis Kit and KOD-Plus-Neo Kit were from TOYOBO (Osaka, Japan). Ni^{2+}-NTA Superflow resin was purchased from Qiagen Inc. (Hilden, Germany). [α-^{32}P]GTP (BLU506H) was obtained from Perkin Elmer Inc. (Waltham, MA, USA). Protein standard markers, T4 DNA ligase, restriction endonucleases, T4 polynucleotide kinase, Dynabeads Protein G, Lipofectamine 2000, Lipofectamine RNAiMAX, 4′,6-diamidino-2-phenylindole (DAPI), MitoTracker, Alexa Fluor 488-conjugated secondary antibody, Sf-900™ II SFM, TRIzol Reagent, Grace's Insect Medium (unsupplemented), and Cellfectin™ II Reagent were obtained from Thermo Scientific (Waltham, MA, USA). Amicon Ultra 15 ml centrifugal concentrators (cutoff 30 kDa) and polyethyleneimine cellulose plates were purchased from Merck (Germany). PrimeScript RT Master Mix, TALON metal affinity resin and Yeastmaker Yeast Transformation System 2 were obtained from Takara (Japan). The DNA fragment rapid purification kit and a plasmid extraction kit were obtained from Magen (Shanghai, China). 2 × T5 Fast qPCR Mix and oligonucleotide primers were obtained from Tsingke (Shanghai, China). Competent *E. coli* DH10Bac was purchased from Weidi Biotechnology (Shanghai, China).

Antibodies

The N-terminal region of hGTPBP3-Iso7 (S^{18}-V^{34}) was used as an epitope to raise rabbit polyclonal antibodies against hGTPBP3-Iso7. The recombinant hGTPBP3 protein (T^{21}-K^{492}) purified from *E. coli* was used as an antigen to generate anti-hGTPBP3 antibody (Abclonal, China). Anti-Myc (M4439), anti-FLAG (F1804), anti-GAPDH (G9295), HRP-labeled anti-mouse and anti-rabbit secondary antibodies were obtained from Sigma-Aldrich (St. Louis, MO, USA). Anti-MTO1 (15650-1-AP), anti-HA (66006-2-Ig), anti-His_6 (66005-1-Ig) and anti-VDAC1 (55259-1-AP) antibodies were obtained from Proteintech (Rosemont, IL, USA). Anti-*E. coli* leucyl-tRNA synthetase (*Ec*LeuRS) was described in a previous study (38).

Gene cloning, mutagenesis, expression and protein purification

Genes encoding the hGTPBP3 precursor were amplified from cDNA obtained from human embryonic kidney 293T (HEK293T) cells and inserted between the NdeI and XhoI sites of pET28a with an N-terminal His_6 tag to form the pET28a-*hGTPBP3* precursor. The recombinant plasmid was used as the template to construct the N-terminal truncated mutant pET28a-*hGTPBP3-ΔN20*, which encodes the mature form of hGTPBP3 with the mitochondrial targeting sequence (MTS) deleted. Gene mutagenesis was performed according to the protocol provided with the KOD-Plus Mutagenesis Kit. The definition of the G domain and N-terminal domain of hGTPBP3 was based on the crystal structure of *Tm*MnmE (PDB: 1XZP) and sequence alignment. The genes encoding the hGTPBP3 G domain (G^{249}-P^{426}) and ΔN-hGTPBP3 (N^{154}-K^{492}) were amplified by PCR using the pET28a-*hGTPBP3* precursor as a template and ligated into pET28a via the restriction enzymes NdeI and XhoI. The primer sequences are listed in Supplementary Table S1.

All constructs were transformed into *E. coli* Rosetta (DE3) cells for gene expression, which was induced with a final concentration of 100 μM IPTG at 18°C for 10 h. Proteins were purified by TALON metal affinity resin according to the manufacturer's protocol. The purified proteins were dialyzed against storage buffer (50 mM Tris-HCl (pH 8.5), 50 mM NaCl, 100 mM KCl, 5 mM β-ME) and stored at −20°C after mixing with an equal volume of glycerol. The protein concentrations were determined by using the BCA kit.

Insect cell culture, transfection and protein expression

Sf9 and High Five cells were cultured in Sf-900™ II SFM medium at 27°C. The pFastBac-*hGTPBP3* precursor was constructed with a C-terminal His_6 tag for gene expression in insect cells. Recombinant baculovirus was generated following the Bac-to-Bac baculovirus expression system (Invitrogen). Recombinant baculoviruses were generated by transfecting the bacmid in Sf9 cells using Cellfectin™ II Reagent according to the manufacturer's protocol. P1 virus stock was harvested from cell culture medium and used to amplify a higher titer P2 virus stock by infecting Sf9 cells and incubating for 5–6 days at 27°C. The same procedure was used to produce P2 virus stock, which was stored at 4°C, protected from light. Gene expression was performed using High Five cells in Sf-900™ II SFM medium by infecting with P3 virus stock at a 1:200 ratio. Cells were harvested by centrifugation (500 × *g*, 5 min) 60 h after infection, washed in PBS and stored at −80°C.

Determination of the N-terminal sequence of hGTPBP3

High Five cells were disrupted by sonication on ice, and then, the whole lysate was applied to Ni-NTA Superflow resin for hGTPBP3 purification according to the manufacturer's protocol. Proteins were separated by electrophoresis by 10% sodium dodecyl sulfate polyacrylamide gel electrophoresis (SDS-PAGE) and transferred to polyvinylidene fluoride (PVDF) membranes in CAPS transfer buffer (10 mM CAPS, 10% methanol), stained with Ponceau red for 25 min and washed with ultrapure water. The washing steps were repeated several times until the band of interest was clearly visible. This band was cut and sent to

Applied Protein Technology (Shanghai, China) to identify the N-terminal sequence through the Edman degradation method.

Measurement of kinetic parameters

The kinetic parameters of hGTPBP3 and its various mutants were measured in a reaction mixture containing 50 mM Tris–HCl (pH 8.0), 300 mM KCl, various concentrations of [α-^{32}P]GTP, and 15 mM $MgCl_2$ at 37°C. Reactions were initiated by the addition of 5 μM hGTPBP3. Two-microliter aliquots at specific time points were quenched in 4 μl of stop solution containing 20 mM GTP, 20 mM EDTA and 1% SDS, and then, 1.5 μl of the quenched aliquots was spotted onto polyethyleneimine cellulose plates pre-washed with water. Thin-layer chromatography (TLC) was performed in 0.5 M formic acid and 0.5 M LiCl to separate [α-^{32}P]GTP and [α-^{32}P]GDP. The plates were visualized by phosphorimaging, and the data were analyzed using Multi Gauge Version 3.0 software (FUJIFILM). Quantification of [α-^{32}P]GDP in comparison with [α-^{32}P]GTP samples of known concentrations was achieved by densitometry.

Cell transfection, immunoprecipitation (IP) and western blot

The coding sequence of the hGTPBP3 precursor was inserted into pCMV-3Tag-3A with a C-terminal 3*FLAG tag and pCMV-3Tag-4A with a C-terminal 3*c-Myc tag. The gene encoding human MTO1 (hMTO1) was recombined into pcDNA3.1 with a C-terminal FLAG tag. HEK293T cells were transfected by using the Lipofectamine 2000 transfection reagent according to the manufacturer's protocol. After transfection for 24 h, the cells were lysed in 500 μl of RIPA buffer (50 mM Tris–HCl (pH 7.5), 150 mM NaCl, 0.5% sodium deoxycholate, 1% Triton X-100, 0.1% SDS) supplemented with a protease inhibitor cocktail for 45 min. The supernatant was collected using centrifugation at 12 000 × *g* for 10 min. All procedures were performed in an ice bath. The supernatant was incubated with the corresponding primary antibody overnight at 4°C, and then, the mixture was incubated with Dynabeads Protein G for 2 h. The beads were washed with PBST (PBS with 0.05% Tween-20) three times. Proteins were eluted in 2× SDS loading buffer [100 mM Tris–HCl (pH 6.8), 4% sodium dodecyl sulfate, 0.2% bromophenol blue, 50% glycerol and 5 mM β-ME] and then subjected to western blot analysis.

Proteins were separated by 10% SDS-PAGE and then transferred onto a PVDF membrane. The PVDF membrane was blocked with 5% (w/v) nonfat dried milk for 1 h at room temperature and incubated with the corresponding primary antibodies overnight at 4°C. Membranes were incubated with HRP (horseradish peroxidase)-conjugated secondary antibody at room temperature for 1 h. The image was obtained using an Amersham Imager 680 (GE, CA, USA).

Immunofluorescence

HEK293T cells were transfected with specific plasmids. After 24 h, cells were stained with MitoTracker for 25 min and then fixed in 4% paraformaldehyde containing PBS for 30 min at room temperature. Fixed cells were blocked in PBS plus 0.1% Triton X-100 buffer containing 5% BSA and incubated with the primary antibody overnight at 4°C. The cells were immunostained with Alexa Fluor 488-conjugated secondary antibody in PBS for 2 h and the nuclear counterstain DAPI for 5 min at room temperature. Fluorescence images were captured with a Leica TCS SP8 STED confocal microscope.

Gel filtration chromatography

Purified mature hGTPBP3 from *E. coli* was analyzed using a Superdex 200 10/300 GL column in running buffer containing 50 mM Tris–HCl (pH 8.5), 50 mM NaCl, 100 mM KCl, and 5 mM β-ME. For dimerization analysis, the *Ec*MnmE G domain, hGTPBP3 G domain and ΔN-hGTPBP3 were preincubated with 100 mM KCl and 200 μM GDP, 200 μM GDP or 1 mM GDP ± 1 mM AlF_x (1 mM $AlCl_3$ and 10 mM NaF) for 30 min on ice. *Ec*MnmE G domain and hGTPBP3 G domain were applied on Superdex 75 10/300 GL column; while ΔN-hGTPBP3 was applied on Superdex 200 10/300 GL column in the same running buffer as mature hGTPBP3, respectively.

Mitochondria isolation

Mitochondria were isolated according to protocols that have been previously described (39). The isolated mitochondria were lysed in RIPA buffer supplemented with a protease inhibitor cocktail. The supernatant was collected and centrifuged at 12 000 × *g* for 10 min, treated with 5× SDS loading buffer and boiled for 10 min at 99°C. The prepared samples were used for Western blot.

Yeast complementation

Genes encoding the hGTPBP3 precursor and its mutants were ligated into p425TEF (40). All constructs were transformed into the *Saccharomyces cerevisiae MSS1* knockout strain (*ScΔMSS1*) by using the Yeastmaker Yeast Transformation System 2 according to the manufacturer's protocol. Transformants were selected on SD/Leu$^-$ plates, and a single clone was cultured in liquid SD/Leu$^-$ medium at 30°C. The culture was diluted to a concentration equivalent to 1 OD_{600}, and a 10-fold dilution series of the yeasts were plated onto YPG [1% yeast extract, 2% peptone, 3% (v/v) glycerol] plates. Complementation was observed by comparing the growth rates of *ScΔMSS1* expressing native hGTPBP3 and its mutants. Yeast transformants were grown in liquid SD/Leu$^-$ at 30°C and lysed following a previously described method (41).

Reverse transcription (RT)-PCR and quantitative real-time PCR (qPCR)

Total RNA was extracted from HEK293T cells using TRIzol Reagent. cDNAs were reverse-transcribed using PrimeScript RT Master Mix according to the manufacturer's protocol. qPCR was carried out using 2 × T5 Fast qPCR Mix kits on a LightCycler 96 (Roche Diagnostics) instrument. The data were normalized against GAPDH expression, and

relative expression was calculated using the ΔΔCT method (42) to compare the expression of hGTPBP3 (isoform 4 and isoform 5) and hGTPBP3-Iso7. qPCR primer sequences are listed in Supplementary Table S1.

siRNA knockdown

siRNA against hGTPBP3-Iso7 and scramble control were obtained from GenePharma (Shanghai, China). siRNA knockdown experiments were carried out using Lipofectamine RNAiMAX (Invitrogen) according to the manufacturer's instructions. HEK293T cells were transfected with the individual siRNA at 20 μM using Lipofectamine RNAiMAX at a 1:2 ratio. After 72 h, transfected cells were validated for knockdown by western blot and qPCR. siRNA sequences are listed in Supplementary Table S1.

RESULT

Identification of the mature form of hGTPBP3

Most nuclear gene-encoded mitochondrial proteins harbor an N-terminal MTS (43). Full-length hGTPBP3 consists of 492 amino acid residues (37). Primary sequence analysis with various eukaryotic GTPBP3/MSS1 proteins or bacterial MnmEs showed that, in comparison with bacterial MnmEs (e.g. *Ec*MnmE, *Tm*MnmE), hGTPBP3 indeed contains an N-terminal extension (Supplementary Figure S2). Considering the localization of hGTPBP3 in mitochondria (34), we suggested that full-length hGTPBP3 likely harbors an N-terminal MTS in the extension, similar to mitochondrial aminoacyl-tRNA synthetases (44). To identify the potential MTS, the hGTPBP3 gene was expressed with a C-terminal His_6 tag using a Bac-to-Bac baculovirus expression system. The protein was purified by Ni-NTA affinity chromatography (Supplementary Figure S3A), and the band separated by SDS-PAGE was transferred onto a PVDF membrane, stained with Ponceau S, excised and subjected directly to automatic Edman degradation in a gas-phase protein sequencer (Supplementary Figure S3B). Protein sequencing analysis showed that the N-terminal sequence of mitochondrial hGTPBP3 was TRRSS, clearly establishing that full-length hGTPBP3 was likely cleaved between C^{20} and T^{21} (Supplementary Figure S2) when it was imported into mitochondria. Therefore, full-length hGTPBP3 and hGTPBP3 with the 20 N-terminal amino acid residues truncated represented the precursor and mature forms of hGTPBP3, designated hereafter as the hGTPBP3 precursor and hGTPBP3, respectively. Then, the gene encoding hGTPBP3 was expressed in *E. coli* and successfully purified to high homogeneity (Figure 1A).

*Ec*MnmE and *Tm*MnmE are homodimers (33). To study the quaternary structure of hGTPBP3, it was subjected to gel filtration analysis. The results showed that hGTPBP3 eluted with a single peak (Figure 1B), corresponding to an observed molecular mass of 151 kDa (Figure 1C). The theoretical molecular mass of purified hGTPBP3 with an N-terminal His_6 tag is 52 kDa, indicating that hGTPBP3 exists as a dimer in solution. Notably, the observed molecular mass of hGTPBP3 is larger than expected, likely due to the elongated shape of the dimer, which has been suggested for *Tm*MnmE, which also exhibits a larger-than-expected observed molecular mass (35). In addition, coimmunoprecipitation (Co-IP) was performed in HEK293T cells. The genes encoding the hGTPBP3 precursor with a C-terminal Myc tag (hGTPBP3-Myc) and with a C-terminal FLAG tag (hGTPBP3-FLAG) were co-expressed in HEK293T cells, and then, cell lysates were immunoprecipitated with anti-FLAG antibodies. Western blot analysis showed that hGTPBP3-Myc coprecipitated with hGTPBP3-FLAG (Figure 1D), suggesting that hGTPBP3 is a homodimer *in vivo*.

MnmG and MnmE form an α2β2 heterotetrameric complex in *E. coli* (17). Similarly, MTO1 and MSS1 form a stable complex in the mitochondria of *S. cerevisiae* (45). Overexpressed hGTPBP3 has been copurified with overexpressed FLAG-tagged hMTO1 (hMTO1-FLAG) (19). To explore whether endogenous hGTPBP3 and hMTO1 interact with each other *in vivo*, we prepared an hGTPBP3 antibody (anti-hGTPBP3) using purified hGTPBP3 as an antigen, which was able to specifically recognize exogenously expressed hGTPBP3 in *E. coli* (Supplementary Figure S3C) and endogenous hGTPBP3 in HEK293T cells (Supplementary Figure S3D). Using an anti-hGTPBP3 antibody in Co-IP, we confirmed that endogenous hMTO1 was indeed coprecipitated (Figure 1E). Accordingly, genes encoding hGTPBP3-Myc and hMTO1-FLAG were co-expressed in HEK293T cells, and Co-IP results showed that hGTPBP3-Myc was pulled down by hMTO-FLAG (Figure 1F).

Collectively, we defined MTS of the hGTPBP3 precursor, purified hGTPBP3 with high purity and revealed that hGTPBP3 is dimeric and interacts with hMTO1 *in vivo*.

hGTPBP3 has intrinsic GTPase activity

A previous study reported that the hGTPBP3 precursor fused with GST (GST-hGTPBP3 precursor) has nearly no GTPase activity (37). To determine the GTP hydrolysis activity of our purified hGTPBP3, we initially optimized the reaction conditions for GTP hydrolysis by this enzyme based on TLC using [α-^{32}P]GTP. Other factors remained constant as the concentration of one component was changed. The pH values ranged from pH 7.0–9.0 with intervals of 0.5, and we found that the observed k_{cat} value peaked at pH 8.0 (Supplementary Figure S4A). In parallel, in the presence of 300 mM KCl or 15 mM $MgCl_2$, the maximal observed k_{cat} value was observed (Supplementary Figure S4B). Thus, the optimal reaction was carried out in buffer containing 50 mM Tris–HCl (pH 8.0), 300 mM KCl, and 15 mM $MgCl_2$ at 37°C for subsequent hGTPBP3 activity determination. The GTPase kinetic parameters showed that the k_{cat} value ($1.49 \pm 0.06\ min^{-1}$) of hGTPBP3 for GTP was nearly 20-fold higher than that ($0.076 \pm 0.008\ min^{-1}$) of the GST-hGTPBP3 precursor (37) (Table 1), while its K_m value (9.5±1.5 μM) was approximately 26-fold lower than that (250 μM) of the GST-hGTPBP3 precursor (37). Therefore, the catalytic efficiency (k_{cat}/K_m) of hGTPBP3 (156.84 $min^{-1}\ mM^{-1}$) was more than 500-fold higher than that of the GST-hGTPBP3 precursor (0.30 $min^{-1}\ mM^{-1}$).

Our data clearly revealed that hGTPBP3 possesses intrinsic GTP hydrolysis activity and is a GTPase.

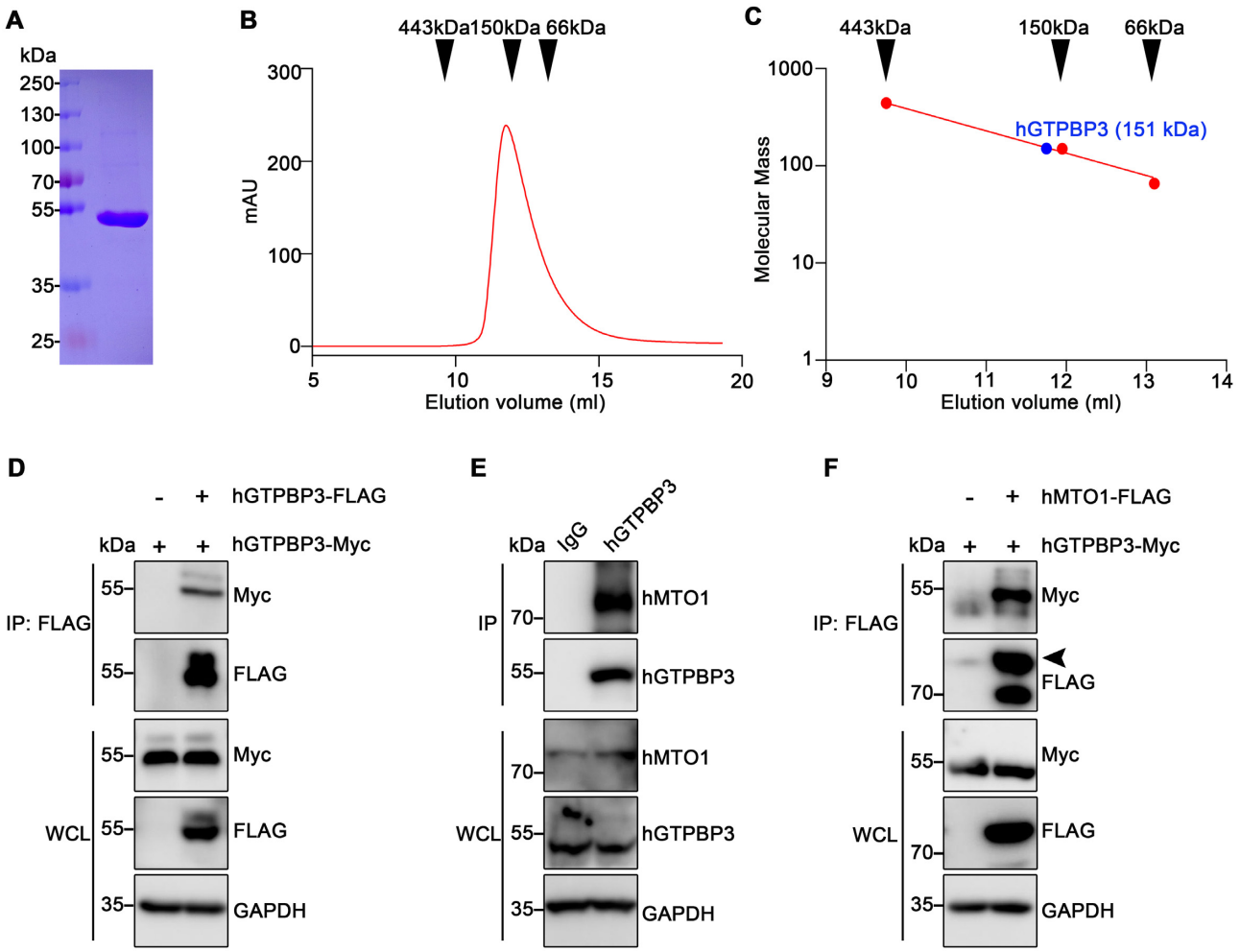

Figure 1. hGTPBP3 is a dimer and interacts with hMTO1. (**A**) SDS-PAGE analysis of purified mature hGTPBP3 from *E. coli*. The protein was stained with Coomassie blue. (**B**) Gel filtration analysis of purified mature hGTPBP3, with the elution volumes of standard proteins of known molecular weight indicated. The three standard proteins were apoferritin (443 kDa), yeast alcohol dehydrogenase (150 kDa) and bovine serum albumin (66 kDa). (**C**) Determination of the molecular mass of mature hGTPBP3 based on the elution volumes of the abovementioned standard proteins. (**D**) The hGTPBP3-FLAG and hGTPBP3-Myc genes were coexpressed in HEK293T cells. hGTPBP3-FLAG was precipitated by hGTPBP3-Myc in a Co-IP assay. (**E**) Endogenous hMTO1 was coprecipitated with endogenous hGTPBP3 by anti-hGTPBP3 but not rabbit IgG. (**F**) The hGTPBP3-Myc and hMTO1-FLAG genes were coexpressed in HEK293T cells. hGTPBP3-Myc was coprecipitated with hMTO1-FLAG in a Co-IP assay. The black arrow indicated hMTO1-FLAG.

The isolated G domain and hGTPBP3 with the N-terminal domain truncated (ΔN-hGTPBP3) exhibited very low catalytic efficiency due to high K_m values

The isolated G domain (G^{216}–G^{384}, calculated molecular weight 18.3 kDa) from *Ec*MnmE exhibits potassium ion-dependent GTPase activity that is nearly identical to the GTPase activity of full-length *Ec*MnmE (33). Similarly, *Ec*MnmE with the N-terminal domain truncated (ΔN-*Ec*MnmE) also retained full potassium ion-dependent GTPase activity (33). However, the isolated G domain of hGTPBP3 has been shown to be inactive (37). We purified the isolated G domain (G^{249}–P^{426}, calculated molecular weight 18.3 kDa) and ΔN-hGTPBP3 (N^{154}-K^{492}, calculated molecular weight 36.1 kDa) (Figure 2A), and then, their GTPase activity was assayed. Kinetics analysis showed that the K_m values of the G domain or ΔN-hGTPBP3 were significantly elevated to 216.7 ± 15.2 or 262.2 ± 17.3 μM, respectively, in comparison with that (9.5 ± 1.5 μM) of hGTPBP3. Moreover, the k_{cat} value of the G domain or ΔN-hGTPBP3 decreased significantly to 0.40 ± 0.06 or 0.76 ± 0.01 min^{-1}, respectively, in comparison with that (1.49 ± 0.06 min^{-1} mM^{-1}) of hGTPBP3. Thus, the catalytic efficiency of the G domain or ΔN-hGTPBP3 was only 2.9% or 4.6% that of hGTPBP3 (Table 1).

For a more direct comparison, we selected two absolutely conserved amino acid residues in the active sites of hGTPBP3 based on the *Ec*MnmE G domain structure (PDB: 2GJ8) (33). *Ec*MnmE N226 (hGTPBP3 N259 counterpart) is a completely conserved site (Figure 2B) in the G domain that binds directly with potassium (Figure 2C), which is essential for catalytic function (33). The absolutely conserved residue E282 of *Ec*MnmE (hGTPBP3 E315 counterpart) (Figure 2B) is considered to be important for GTP hydrolysis by stabilizing the attacking water in the G domain (33). Mutation of N226 or E282 to Ala drastically reduced the GTP hydrolysis

Table 1. Kinetic parameters of the GTPase activity of hGTPBP3, G domain, ΔN-hGTPBP3 and the hGTPBP3 mutants for GTP

	Enzyme	K_m (μM)	k_{cat} (min^{-1})	k_{cat}/K_m ($min^{-1}mM^{-1}$)	Relative k_{cat}/K_m (%)
Wild type	hGTPBP3	9.5 ± 1.5	1.49 ± 0.06	156.84	100
	G domain	216.7 ± 15.2	0.40 ± 0.06	1.85	2.9
	ΔN-hGTPBP3	262.2 ± 17.3	0.76 ± 0.01	2.90	4.6
	N259A	11.4 ± 3.6	0.07 ± 0.01	6.51	4.2
	E315A	11.9 ± 3.1	0.07 ± 0.02	5.58	3.6
N-terminal domain	E142K/R136E	15.1 ± 0.6	0.52 ± 0.03	34.44	21.9
Helical domain	E159V	26.1 ± 2.7	0.75 ± 0.14	28.87	18.4
	E159R/R431E	12.1 ± 1.9	1.55 ± 0.04	128.11	81.7
	A162P	91.0 ± 10.5	0.93 ± 0.12	10.19	8.9
	E225K/A322P	37.8 ± 12.5	0.79 ± 0.12	21.00	13.4
	E459K	12.0 ± 2.2	1.69 ± 0.24	140.62	89.7
G domain	P257H	101.5 ± 27.5	0.49 ± 0.07	4.81	3.1
	ΔG312-V319	50.5 ± 5.6	0.50 ± 0.05	9.99	6.4
	A322P	91.3 ± 5.9	0.45 ± 0.05	4.90	3.1

The results are the averages of three independent measurements with the standard deviations indicated.

rate of *Ec*MnmE (33). Hence, we constructed hGTPBP3-N259A and hGTPBP3-E315A mutants, and kinetics analysis of these mutants showed that they exhibited 3.6% and 4.2% catalytic efficiency, respectively, compared with that of hGTPBP3, mainly resulting from the strong decrease in k_{cat} and a small increase in K_m (Table 1). These data clearly showed that the G domain and ΔN-hGTPBP3 exhibited very low GTPase catalytic efficiency, which was comparable to those of two inactive hGTPBP3 mutants.

Dimerization is a prerequisite for active GTP hydrolysis by the isolated G domain of *Ec*MnmE (33). Considering the very low GTPase activity of the isolated hGTPBP3 G domain, we explored whether the inactive hGTPBP3 G domain forms a dimer in the presence of potassium and the transition state mimic GDP-AlF_x, which has been observed for the *Ec*MnmE G domain or ΔN-*Ec*MnmE (33). For a direct comparison, we purified the *Ec*MnmE G domain (G^{216}–G^{384}). Indeed, the *Ec*MnmE G domain formed a dimer (38.7 kDa) in the presence of potassium and 200 μM GDP-AlF_x in the gel filtration analysis, consistent with previous results (Figure 2D) (33). We subsequently analyzed the dimerization of the hGTPBP3 G domain and ΔN-hGTPBP3. In the presence of potassium and 200 μM GDP, the isolated G domain of hGTPBP3 eluted as a slightly elongated monomer (24.7 kDa) (Figure 2E), and ΔN-hGTPBP3 also eluted as an elongated monomer (67 kDa) (Figure 2F). However, both hGTPBP3 G domain (25.6 kDa) and ΔN-hGTPBP3 (65 kDa) failed in efficient dimerization in the presence of potassium and 200 μM GDP-AlF_x (Figure 2E, F), in contrast to the *Ec*MnmE G domain (Figure 2D). We subsequently elevated the concentration of GDP-AlF_x to 1 mM. Indeed, hGTPBP3 G domain (39 kDa) or ΔN-hGTPBP3 (119 kDa) obviously formed a dimer under such condition (Figure 2E, F). The molecular weight of dimeric ΔN-hGTPBP3 (119 kDa) was nearly the same with the dimeric ΔN-*Ec*MnmE (115 kDa) (33). These results indicated that low concentration of GTP is less efficient at inducing dimerization of the hGTPBP3 G domain or ΔN-hGTPBP3, which likely explains the low GTPase activity of the isolated hGTPBP3 G domain or ΔN-hGTPBP3.

Multiple structural and/or functional defects due to pathogenic mutations of hGTPBP3

Previously, several homozygous or compound heterozygous single-point (R3L, E142K, E159V, A162P, P257H, A322P, D337H and E459K), double-point (E225K/A322P) or deletion (ΔG312-V319) mutations were linked to mitochondrial disorders with a phenotype of hypertrophic cardiomyopathy, lactic acidosis, and encephalopathy, with unclear mechanisms (28). Purification of active hGTPBP3 provides a solid foundation for elucidation of its potential molecular defect in GTPase activity. Among the above sites, R3 is located in the MTS; E142 is in the N-terminal domain; E159, A162, E225 and E459 are situated in the helical domain, which is proposed to interact with hMTO1 based on the SAXS model (46); and the remaining residues, namely, P257, G312-V319, A322 and D337, are in the G domain (Figure 3A).

Genes encoding the hGTPBP3 precursor and the above mutants were initially expressed in HEK293T cells with a C-terminal FLAG tag. Western blot analysis using the whole cell lysate (WCL) showed that the steady-state protein levels of hGTPBP3-R3L, hGTPBP3-E142K, hGTPBP3-E159V, hGTPBP3-P257H and hGTPBP3-D337H decreased significantly, while those of other mutants were comparable with that of wild-type hGTPBP3 (Figure 3B). Mitochondria were then isolated from the cells, and the abundance of the above five mutants was also found to be decreased (Figure 3C). Decreased amounts of hGTPBP3-R3L, hGTPBP3-E142K, hGTPBP3-E159V, hGTPBP3-P257H and hGTPBP3-D337H in WCL and mitochondrial fractions suggested that these mutants impaired protein structure and/or stability. To determine whether these proteins were subsequently degraded *in vivo* and the potential degradation pathway, hGTPBP3 precursor, hGTPBP3-R3L, hGTPBP3-E142K, hGTPBP3-E159V, hGTPBP3-P257H and hGTPBP3-D337H were overexpressed in HEK293T cells, which were treated with MG132, a proteasome inhibitor (47), and leupeptin, a lysosomal inhibitor (48), respectively. The results showed that the abundance of all the mutants increased significantly with MG132 treatment (Figure 3D), while that of hGTPBP3 precursor increased only slightly (Figure

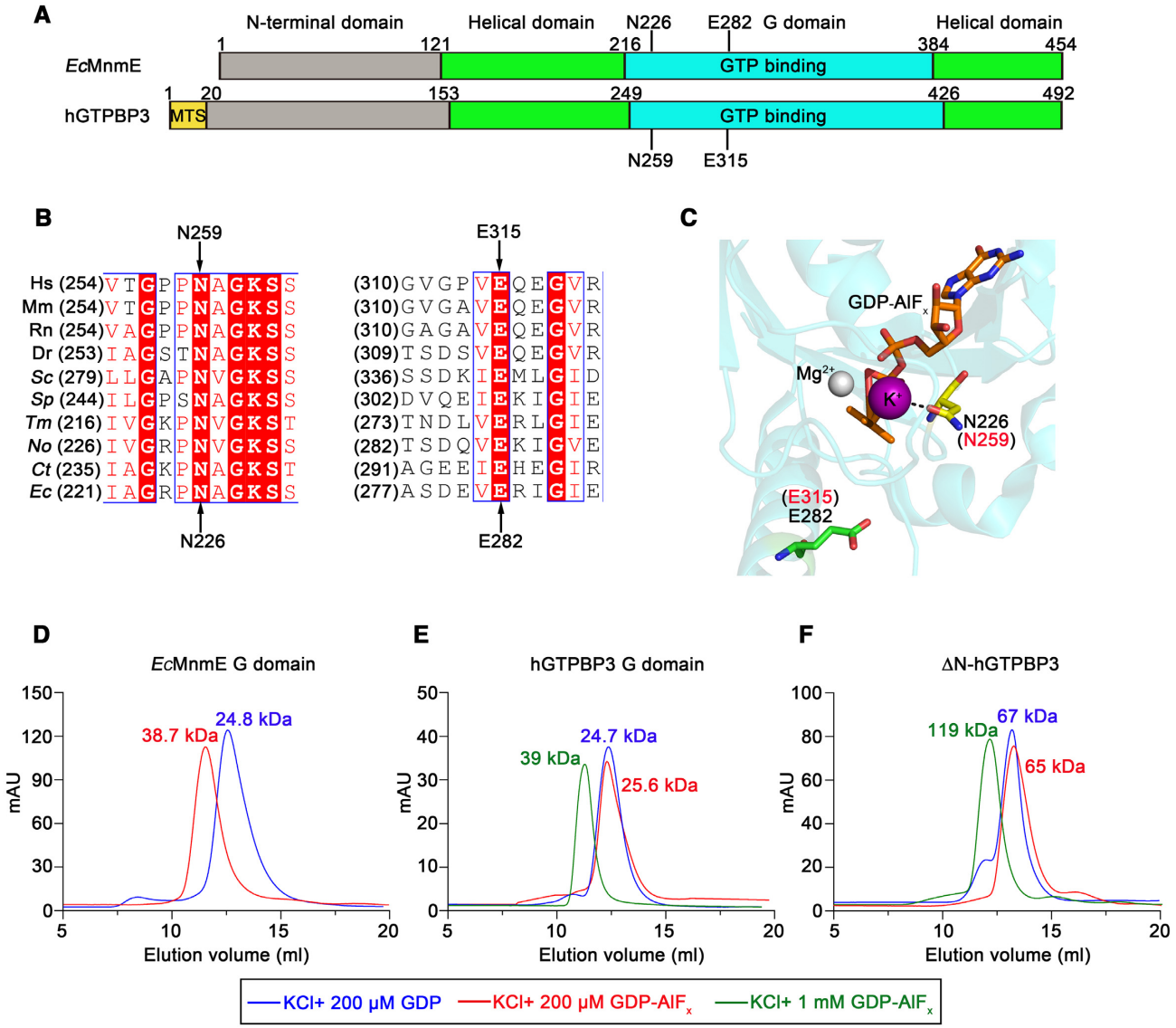

Figure 2. The hGTPBP3 G domain and ΔN-hGTPBP3 exhibited very low GTPase activity. (**A**) Schematic diagram showing the domain compositions of hGTPBP3 and *Ec*MnmE based on the crystal structure of *Tm*MnmE (PDB: 1XZP). The N-terminal domain (gray), helical domain (green), and G domain (cyan) were indicated. (**B**) Primary sequence alignment of MnmE/MSS1/GTPBP3 in different species. The amino acid residues N259 and E315 of hGTPBP3 and N226 and E282 of *Ec*MnmE were indicated by black arrows. Mm, *Mus musculus*; Rn, *Rattus norvegicus*; Hs, *Homo sapiens*; Dr, *Danio rerio*; *Tm*, *Thermotoga maritima*; *No*, Nostoc sp.; *Ct*, *Chlorobaculum tepidum*; *Ec*, *Escherichia coli*; *Sc*, *Saccharomyces cerevisiae*; *Sp*, *Schizosaccharomyces pombe*. (**C**) 3D model of the hGTPBP3 G domain based on the *Ec*MnmE G domain structure (PDB: 2GJ8). N259 (red) and E315 (red) are essential for GTPase activity. GDP-AlF$_x$ (orange), K^+ (pink), and Mg^{2+} (gray) were displayed. Note that *Ec*MnmE counterparts (N226 and E282) were shown in black. (**D-F**) Gel filtration analysis of the multimerization behavior of the *Ec*MnmE G domain (**D**), hGTPBP3 G domain (**E**) and ΔN-hGTPBP3 (**F**). Purified protein was preincubated with 100 mM KCl and 200 μM GDP or 200 μM GDP-AlF$_x$, 1 mM GDP-AlF$_x$ for 30 min on ice. Apparent molecular masses corresponding to elution volumes were indicated.

3D); however, leupeptin treatment had no obvious influence on the steady-state protein levels of these mutants and hGTPBP3 precursor (Figure 3D). These results suggested that the decrease in the amounts of the above mutants was likely due to proteasome-dependent degradation. To further confirm that these mutants were ubiquitylated, each of the five mutants was coexpressed with HA-tagged ubiquitin (HA-Ub) and enriched by immunoprecipitation. Indeed, compared with wild-type hGTPBP3, these mutants were obviously and extensively ubiquitylated (Figure 3E).

To understand the biochemical effects of the mutations, we expressed genes encoding these mutants that excluding MTS (except R3L in the MTS) in *E. coli* to purify them. However, hGTPBP3-E142K and hGTPBP3-D337H could not be obtained because inclusion bodies formed during gene expression in *E. coli*, which is in accordance with their decreased amount in human cells, further confirming their detrimental effect on protein structure. The GTPase activities of the other seven mutants were assayed (Table 1). Analysis of the kinetic parameters of GTP hydrolysis showed that the K_m values of all mutants, except hGTPBP3-E459K,

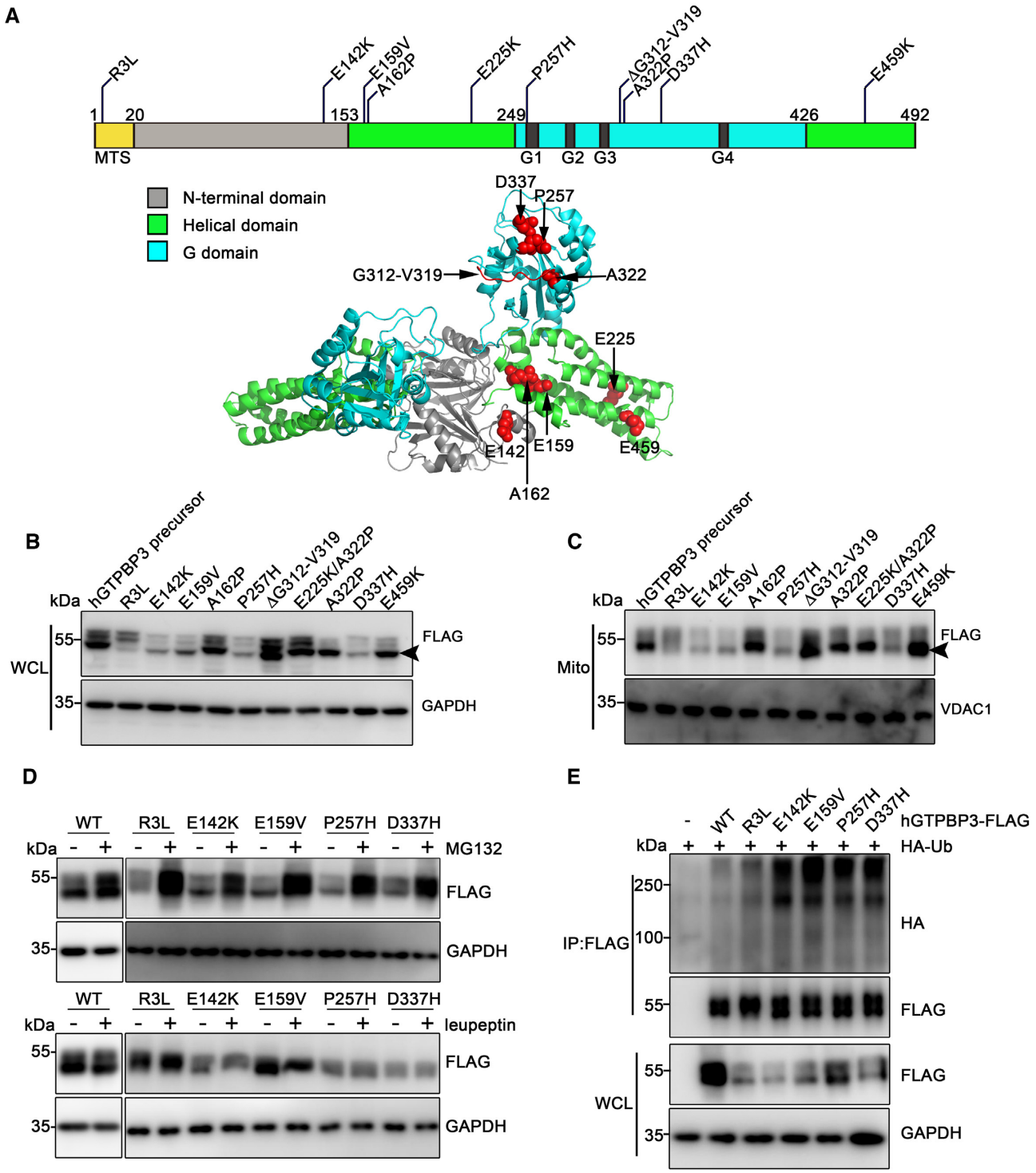

Figure 3. Multiple structural and/or functional defects due to pathogenic mutations of hGTPBP3. (**A**). Localization of pathogenic mutations in hGTPBP3 domains (upper panel) or in the dimeric structure of *Tm*MnmE (PDB: 1XZP) (lower panel) was observed. Mutant residues and the G312-V319 region were indicated in red. Gray, the N-terminal domain; green, the helical domain; cyan, the G domain. (**B**) Detection of the steady-state protein level after overexpression of genes encoding hGTPBP3 and ten mutants using an anti-FLAG antibody in WCL of HEK293T cells. GAPDH was detected as a loading control. The black arrow indicated overexpressed hGTPBP3 precursor and mutants. (**C**) Protein level of hGTPBP3 and mutants in mitochondria (Mito) of HEK293T cells expressing each mutant. VDAC1 was used as a loading control. The black arrow indicated overexpressed hGTPBP3 precursor and mutants. (**D**) Protein levels of hGTPBP3 precursor, hGTPBP3-R3L, hGTPBP3-E142K, hGTPBP3-E159V, hGTPBP3-P257H and hGTPBP3-D337H from HEK293T cells treated with or without 10 μM MG132 (upper panel) and 50 μM leupeptin (lower panel) for 4 h. WT represented the hGTPBP3 precursor. (**E**) hGTPBP3-R3L, hGTPBP3-E142K, hGTPBP3-E159V, hGTPBP3-P257H and hGTPBP3-D337H were extensively ubiquitylated. hGTPBP3 mutants and HA-Ub were coexpressed in HEK293T cells and immunoprecipitated with an anti-FLAG antibody. The ubiquitylation level of each protein was detected using an anti-HA antibody. WT represented the hGTPBP3 precursor.

for GTP were significantly elevated (~3- to 11-fold), while their k_{cat} values decreased modestly (~2- to 3-fold), leading to significantly decreased catalytic efficiency values (3–18% that of wild-type hGTPBP3), most of which were comparable with those of the catalysis-defective hGTPBP3-N259A and hGTPBP3-E315A mutants. However, both the K_m and k_{cat} values of hGTPBP3-E459K were only slightly altered. Therefore, the above data clearly showed that the E159V, A162P, P257H, A322P, E225K/A322P and ΔG312-V319 mutations impaired or abolished the GTPase activity of hGTPBP3, while E459K had little effect on GTP hydrolysis.

To more directly monitor the *in vivo* tRNA modification activity of all mutants, we used a yeast *MSS1* gene knockout strain, *Sc*Δ*MSS1*^{R} (*Sc*Δ*MSS1* for short hereafter) (34), which exhibits a growth defect in respiratory medium using glycerol as a carbon source, suggesting a critical role for the equivalent cmnm^{5}U of yeast mitochondrial tRNAs in mitochondrial translation and homeostasis. We initially confirmed that deletion of *MSS1* caused growth arrest in YPG medium and that overexpression of native hGTPBP3 rescued yeast growth (Figure 4A). However, the type of modification (cmnm^{5}U or τm^{5}U) in yeast mitochondrial tRNAs expressing native hGTPBP3 was currently unclear. Subsequently, all genes encoding the hGTPBP3 precursor, pathogenic mutants, and two inactive hGTPBP3 mutants (hGTPBP3-N259A and hGTPBP3-E315A) were expressed in *Sc*Δ*MSS1*. Western blot analysis showed that all proteins had similar abundances (Figure 4B), in contrast to the differential levels in HEK293T cells (Figure 3B), suggesting that unstable mutants in HEK293T cells, including hGTPBP3-R3L, hGTPBP3-E142K, hGTPBP3-E159V, hGTPBP3-P257H and hGTPBP3-D337H, were not degraded efficiently in yeasts (Figure 4B). The growth of the transformants was observed in both SD/Leu$^-$ and YPG media. The data showed that the hGTPBP3 precursor was able to complement the loss of MSS1 (Figure 4A), suggesting that native hGTPBP3 is able to mediate GTP hydrolysis and tRNA modification *in vivo* in yeasts, in line with previous results (13,34). As expected, catalysis-defective N259A and E315A mutants failed to support yeast growth in YPG medium (Figure 4C), suggesting a crucial role of GTP hydrolysis in tRNA modification *in vivo*.

Among all the mutants, only hGTPBP3-D337H could rescue the growth defect, despite having obviously reduced efficiency compared with that of hGTPBP3 (Figure 4C). Notably, hGTPBP3-D337H was unstable in both human and *E. coli* cells, and its kinetics were not determined because it could not be purified. This result suggested that once stably expressed (Figure 4B), hGTPBP3-D337H likely had the ability to catalyze GTP hydrolysis and mediate tRNA modification *in vivo*. In contrast, all other mutants were unable to support yeast growth, although the protein levels of all the mutants were similar (Figure 4B). Subsequently, we explored whether the mutations modulated the interaction of hGTPBP3 and hMTO1. Genes encoding wild-type hMTO1 and each wild-type hGTPBP3 precursor and its mutants were coexpressed in HEK293T cells. Co-IP analysis showed that the level of coprecipitated hMTO1-Myc was obviously reduced by hGTPBP3-R3L, hGTPBP3-A162P and hGTPBP3-ΔG312-V319 (Figure 4D). Based on *E. coli* MnmE/MnmG SAXS modeling (46), *Ec*MnmE A130 (A162 in hGTPBP3) and D279-I286 (G312-V319 in hGTPBP3) are indeed located close to the MnmE/MnmG interaction interface, suggesting regions containing A162 and G312-V319 are important for the interaction of hGTPBP3 with hMTO1.

We further selected three mutations in the G domain (P257H, ΔG312–V319 and A322P) to explore whether their low GTPase activities were due to impaired dimerization. The isolated G domain containing each of the mutations was purified. Gel filtration analysis showed that the G domain with P257H (Figure 4 E), ΔG312–V319 (Figure 4F) or A322P (Figure 4G) eluted as a monomer (25 kDa) in the presence of potassium and 200 μM GDP. However, they all formed a dimer in the presence of potassium and 1 mM GDP-AlF$_x$ (Figure 4E–G). These results suggested that the low GTPase activities of these mutants were not due to the deficient dimerization ability of G domain.

The R3L mutation blocks hGTPBP3 import into mitochondria

Considering that R3 was located in the MTS, the above results suggested that R3 is likely a critical determinant of the localization of hGTPBP3 into mitochondria. To determine the potential detrimental effect of R3L on mitochondrial targeting, we fused the MTS (M^1-C^{20}) of hGTPBP3 at the N-terminus of EGFP to form MTS$_{hGTPBP3}$-EGFP. Free EGFP was distributed in both the cytoplasm and nucleus (Figure 5A). Indeed, MTS$_{hGTPBP3}$-EGFP was distributed in the mitochondria (Figure 5A), suggesting a high mitochondrial targeting efficiency of hGTPBP3 MTS. However, after introducing the R3L mutation, the resultant MTS$_{hGTPBP3}$-R3L-EGFP was not targeted into mitochondria and was instead located in both the cytoplasm and nucleus (Figure 5A). We further used a yeast model to investigate the effect of R3L on mitochondrial targeting. Previously, we established a 5-fluoroorotic acid (5-FOA)-sensitive *Saccharomyces cerevisiae* chromosomal *MST1* gene (encoding mitochondrial threonyl-tRNA synthetase, *Sc*mtThrRS) knockout strain (*Sc*Δ*MST1*), the survival of which under respiratory conditions critically relies on an MTS (M^1-S^{31}) for targeting *Sc*mtThrRS, which is expressed from a rescue plasmid, into mitochondria (49) (Figure 5B). We replaced the MTS of *Sc*mtThrRS with that of hGTPBP3. As expected, the yeast expressing MTS$_{hGTPBP3}$-*Sc*mtThrRS grew readily on respiratory medium (YPG/5-FOA) (Figure 5B), again suggesting efficient import of mature *Sc*mtThrRS by the hGTPBP3 MTS. After introducing the R3L mutation, the yeasts expressing MTS$_{hGTPBP3}$-R3L-*Sc*mtThrRS were able to survive but with a lower efficiency (Figure 5B). The time-course growth curve showed that the growth of yeasts expressing MTS$_{hGTPBP3}$-R3L-*Sc*mtThrRS was lower than that of yeasts expressing MTS$_{hGTPBP3}$-*Sc*mtThrRS (Figure 5C). Taken together, the above results clearly showed that R3L impaired mitochondrial localization in both HEK293T and yeast cells.

The E142-R136 and E159-R431 interactions are critical for hGTPBP3 structure and function

We next focused on four other unstable mutants, including hGTPBP3-E142K, hGTPBP3-E159V, hGTPBP3-

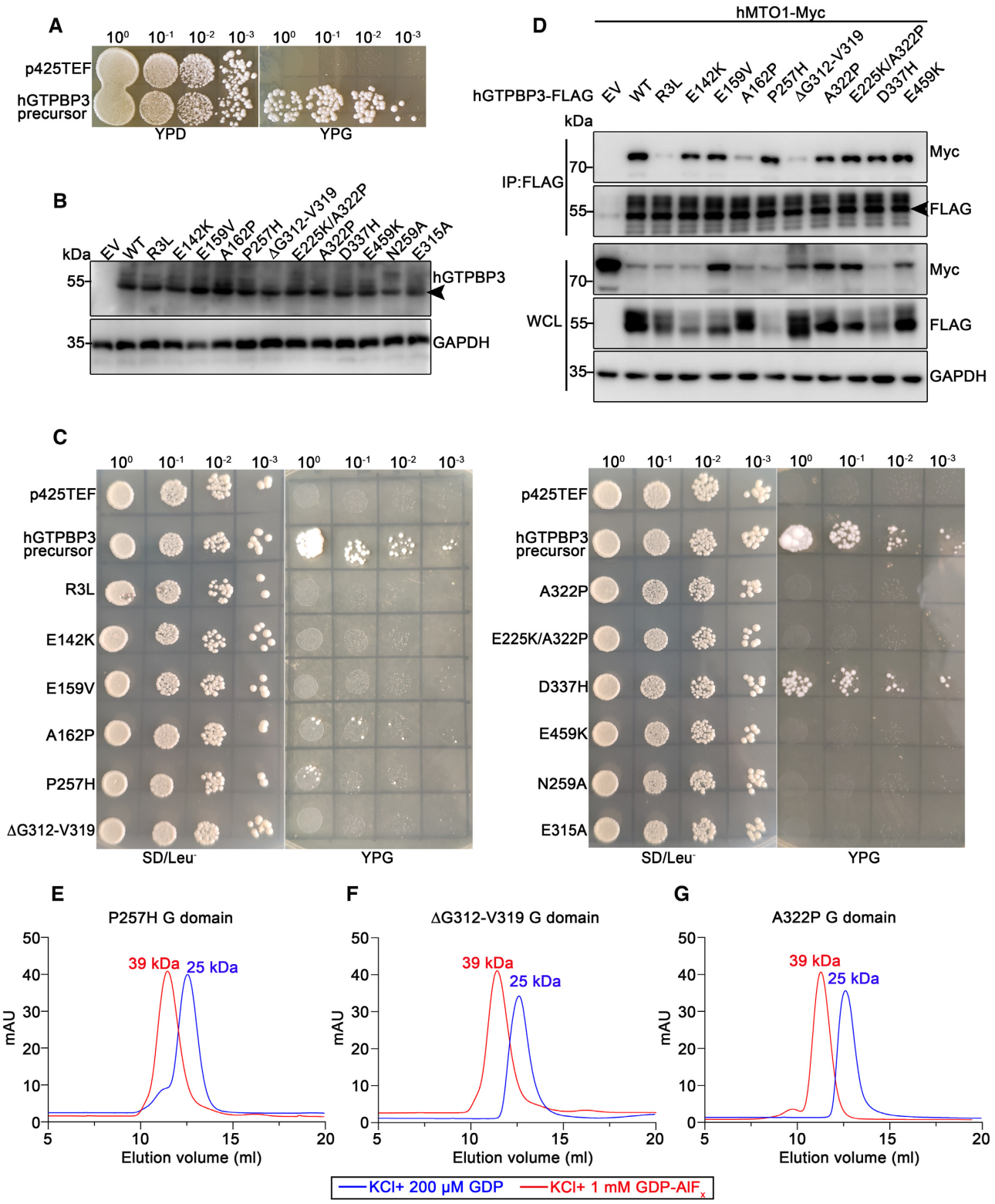

Figure 4. Analysis of hGTPBP3 pathogenic mutants *in vivo.* (**A**) Complementation phenotype of the hGTPBP3 precursor using the *Sc*Δ*MSS1* strain in the YPD or YPG plates. The empty vector p425TEF was introduced as a negative control. (**B**) Protein level of hGTPBP3 pathogenic mutants in the WCL of yeasts. GAPDH was included as a loading control. The black arrow indicated the hGTPBP3 precursor and mutants. (**C**) Complementation phenotype of hGTPBP3 and its mutants using the *Sc*Δ*MSS1* strain in SD/Leu$^-$ or YPG plates. The empty vector p425TEF and the gene encoding the hGTPBP3 precursor were introduced as negative and positive controls, respectively. (**D**) IP assay to detect the interaction between hGTPBP3 mutants and hMTO1. Ten hGTPBP3 mutants and hMTO1 were coexpressed in HEK293T cells and immunoprecipitated by an anti-FLAG antibody. Coprecipitation of hMTO1 was detected with an anti-Myc antibody. WT represented the hGTPBP3 precursor. The black arrow indicated precipitated hGTPBP3 and mutants. (E–G) Gel filtration analysis of the dimerization of the hGTPBP3 G domain P257H (**E**), ΔG312-V319 (**F**), A322P (**G**). Purified protein was preincubated with 100 mM KCl and 200 μM GDP or 1 mM GDP-AlF$_x$ for 30 min on ice. Apparent molecular masses corresponding to elution volumes were indicated.

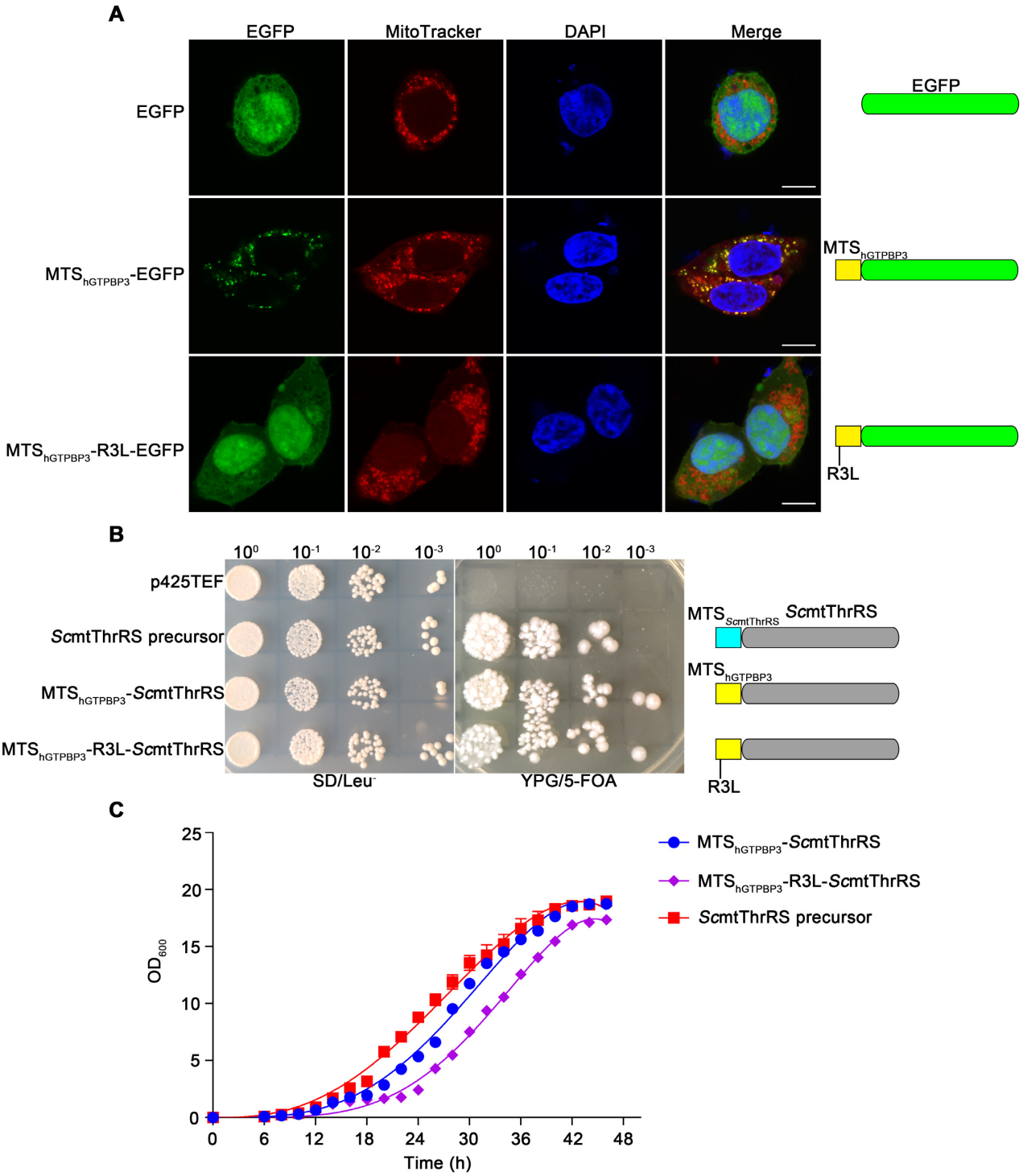

Figure 5. The R3L mutation blocks hGTPBP3 import into mitochondria. (**A**) Cellular localization of overexpressed MTS$_{hGTPBP3}$-EGFP or MTS$_{hGTPBP3}$-R3L -EGFP in HEK293T cells analyzed by fluorescence microscopy. EGFP was included as a control. The schema on the right represented the corresponding composition model. Scale bar: 10 μm. (**B**) Growth phenotypes of yeasts expressing MTS$_{hGTPBP3}$-*Sc*mtThrRS or MTS$_{hGTPBP3}$-R3L-*Sc*mtThrRS using the *Sc*Δ*MST1* strain in YPG/5-FOA plates. p425TEF and the *Sc*mtThrRS precursor were introduced as a negative and positive control, respectively. The schema on the right represented the corresponding composition model. (**C**) Representative yeast growth curves were determined in YPG liquid culture at an initial cell density (OD$_{600}$) of 0.1.

P257H and hGTPBP3-D337H. E142 is a highly conserved site (Figure 6A) in the N-terminal domain in the MnmE/MSS1/GTPBP3 protein family (only D163 in *Sc*MSS1). Based on the crystal structure of *Tm*MnmE (PDB: 1XZP), R101 of *Tm*MnmE (R136 in hGTPBP3) has direct interdomain contact with E107 (E142 in hGTPBP3) (Figure 6B, middle panel) via side-chain electrostatic interactions in the N-terminal domain. Notably, R136 of hGTPBP3 is an absolutely conserved residue in all three kingdoms of life (Figure 6A). Based on these observations, we proposed that the hGTPBP3 E142K mutation likely leads to mutual repulsion between K142 and R136 and thus to structural instability (Figure 6B, lower part in left panel). To test this possibility, in the context of hGTPBP3-E142K, we mutated R136 to E to form the double-point mutant hGTPBP3-E142K/R136E. We overexpressed genes encoding the hGTPBP3 precursor and hGTPBP3-E142K/R136E in HEK293T cells. In contrast to the obviously decreased level of hGTPBP3-E142K (Figure 3B), the amount of hGTPBP3-E142K/R136E was restored to nearly the same level as that of the wild type in the WCL and mitochondrial fraction (Figure 6C). In parallel, despite full formation of aggregates in the expression of the hGTPBP3-E142K gene in *E. coli*, the hGTPBP3-E142K/R136E gene was successfully expressed, and the double-point mutant could be purified with a yield similar to that of wild-type hGTPBP3. The kinetic parameters of hGTPBP3-E142K/R136E in GTP hydrolysis were measured, and the results showed that the K_m value was 1.6-fold higher than that of hGTPBP3, while the k_{cat} value decreased 2.8-fold, leading to a catalytic efficiency (k_{cat}/K_m) that was 21.9% that of the native enzyme (Table 1). The yeast complementation assay further confirmed that hGTPBP3-E142K/R136E regained the capacity to complement loss of *MSS1 in vivo*, albeit with a lower efficiency (Figure 6D), and the protein level in yeast was almost the same as that of the wild type (Figure 6E).

With regard to the E159V mutation, we analyzed the location of E159 in the primary sequence of hGTPBP3 and its spatial position based on the tertiary structure of *Tm*MnmE (PDB: 1XZP). Similarly, E159 of hGTPBP3 is analogous to *Tm*MnmE E124, an absolutely conserved amino acid residue (Figure 6A). E159 of hGTPBP3 directly interacts with the side-chain guanidinium group of another highly conserved residue, R431 in the helical domain, and accordingly, there is an electrostatic interaction between E124 and R387 in *Tm*MnmE (Figure 6B, middle panel), implying that this interaction is pivotal to protein structure and function. In hGTPBP3-E159V, the interaction is disrupted by a hydrophobic Val. To understand the importance of the interaction, the hGTPBP3-E159R single-point mutant and hGTPBP3-E159R/R431E double-point mutant were constructed. The protein level of hGTPBP3-E159R was significantly decreased, while that of hGTPBP3-E159R/R431E was restored to half of that of the wild type (Figure 6F). We successfully obtained hGTPBP3-E159R/R431E using an *E. coli* expression system; however, hGTPBP3-E159R formed inclusion bodies during expression in *E. coli*, suggesting a detrimental effect on protein structure in *E. coli*. The GTPase activity of hGTPBP3-E159R/R431E was assayed, and the parameters showed that the K_m value was 1.3-fold higher than that of hGTPBP3, while the k_{cat} value increased slightly. Consequently, the catalytic efficiency was 81.7% that of the native enzyme (Table 1). hGTPBP3-E159R/R431E, but not hGTPBP3-E159R, was able to support yeast growth (Figure 6G), although the abundances of these proteins were similar in yeast (Figure 6H). Together, the above data showed that the interaction between the conserved E142 and R136 and that between E159 and R431 are critical for maintaining local protein structure in different domains and thus contribute to GTPase activity *in vitro* and tRNA modification *in vivo*.

The other two mutations, namely, P257H and D337H, are located in the G domain. P257 is partially conserved, and its counterpart in bacterial MnmE is a basic residue (Lys or Arg) (Figure 6A). In the *Tm*MnmE structure, K219 (P257 in hGTPBP3) is located in a linker connecting two neighboring α-helices and interacts with the side-chain carboxyl group E308 (S345 in hGTPBP3) (Figure 6B), implying an important role of this residue in maintaining protein structure. The results suggested that mutation of such a key residue disturbs the local conformation of the G domain. Indeed, the K_m value of hGTPBP3-P257H increased nearly 11-fold, representing the greatest value among all the mutants tested. D337 is also a conserved site (Figure 6A), and its counterpart in *Tm*MnmE (D300) is immediately downstream of an α-helix and is surface exposed without any interaction with other residues (Figure 6B). The D337H mutation probably leads to subtle alterations in the conformation of the enzyme and to subsequent protein instability in *E. coli* and human cells.

The above analyses determined the various effects of the pathogenic mutations on structure and/or function of hGTPBP3, which were integrated into a comprehensive Table (Table 2) for clarity.

Identification of a new cytoplasm-localized isoform of hGTPBP3

Both the NCBI and UniProt databases suggest the existence of four isoforms of hGTPBP3: isoform 3 with 471 amino acid residues, isoform 4 with 524 residues, isoform 5 (regarded as the canonical wild-type hGTPBP3 precursor) with 492 residues, and isoform 7 with 514 residues (Figure 7A). Isoform 7 (designated hGTPBP3-Iso7 hereafter) was the most unique because it harbors a completely distinct N-terminus (M^1-A^{40}) compared to that of the other three isoforms (M^1-R^{18}) (Figure 7A). Notably, the fragment encompassing M^1-C^{20} functions as the MTS for the hGTPBP3 precursor. Indeed, Mitoprot (https://ihg.gsf.de/ihg/mitoprot.html) predicts no mitochondrial localization of hGTPBP3-Iso7. This observation suggested that the cellular localization of hGTPBP3-Iso7 (if expressed) may be distinct from that of the hGTPBP3 precursor.

Two primers (Iso7-F and Iso7-R), encompassing the whole open reading frame (ORF) of database-reported hGTPBP3-Iso7 (514 aa), were designed to amplify *hGTPBP3-Iso7* from HEK293T cDNA, which was indeed amplified and then inserted into pET28a (Supplementary Figure S5A). DNA sequences from 10 selected clones showed that all the amplified ORFs contained 1482 bp, encoding a 493-aa protein. These data clearly showed that hGTPBP3-Iso7 mRNA existed *in vivo*, despite being

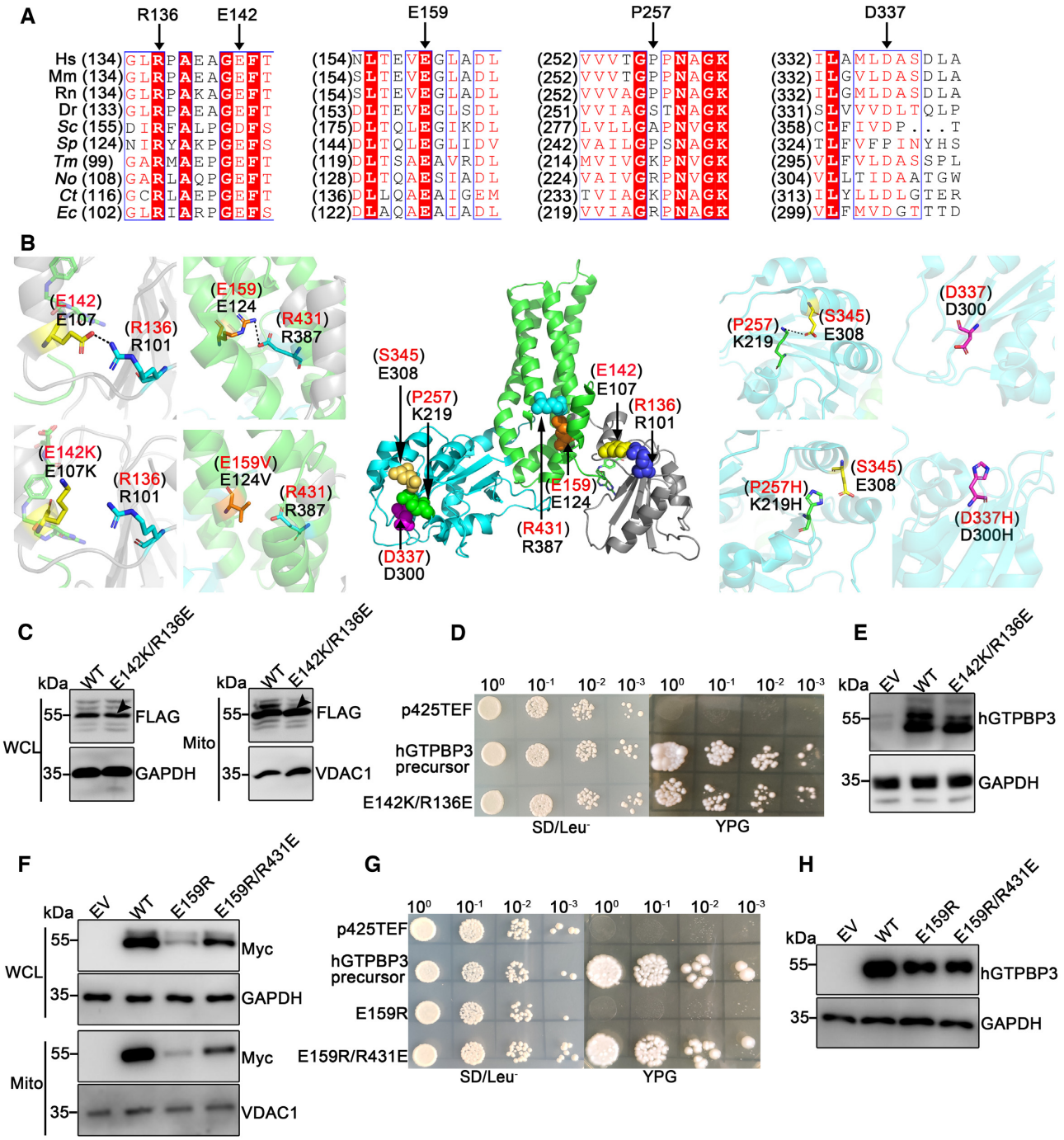

Figure 6. The E142-R136 and E159-R431 interactions are critical for hGTPBP3 structure and function. (**A**) Primary sequence alignment of MnmE/MSS1/GTPBP3 in different species. The amino acid residues E142, E159, P257 and D337 of hGTPBP3 were indicated by black arrows. Mm, *Mus musculus*; Rn, *Rattus norvegicus*; Hs, *Homo sapiens*; Dr, *Danio rerio*; *Tm*, *Thermotoga maritima*; *No*, Nostoc sp.; *Ct*, *Chlorobaculum tepidum*; *Ec*, *Escherichia coli*; *Sc*, *Saccharomyces cerevisiae*; *Sp*, *Schizosaccharomyces pombe*. (**B**) Pairwise comparisons between the wild-type (top) and mutant (bottom) residues for predicted changes in local contacts with other amino acids based on the crystal structure model of *Tm*MnmE (PDB: 1XZP). Amino acids (black and red are *Tm*MnmE and hGTPBP3 residues, respectively) were indicated. (**C**) Protein level of overexpressed hGTPBP3-E142K/R136E in WCL or mitochondria of HEK293T cells. The black arrow indicated WT and E142K/R136E. (**D**) Yeast complementation results for hGTPBP3-E142K/R136E in a SD/Leu$^-$ or YPG plate. (**E**) Protein level of hGTPBP3-E142K/R136E in the WCL of yeast transformants. (**F**) Protein levels of hGTPBP3-E159R and E159R/R431E in WCL or mitochondria of HEK293T cells. (**G**) Yeast complementation results for hGTPBP3-E159R and hGTPBP3-E159R/R431E in a SD/Leu$^-$ or YPG plate. (**H**) Protein levels of hGTPBP3-E159R and hGTPBP3-E159R/R431E in the WCL of yeast transformants. WT represented the hGTPBP3 precursor. The empty vector p425TEF and the gene encoding the hGTPBP3 precursor were introduced as a negative or positive control, respectively, in (D) and (G).

Table 2. The effect of mutations of hGTPBP3 to structure and/or function

hGTPBP3 mutants	Stability	Relative GTPase activity (%)	Yeast complementation	The interaction with hMTO1
R3L	+	nm	No	+
E142K	+	nm	No	++
E142K/R136E	++	21.9	Yes	nm
E159V	+	18.4	No	++
E159R	+	nm	No	nm
E159R/R431E	++	81.7	Yes	nm
A162P	++	8.9	No	+
E225K/A322P	++	13.4	No	++
P257H	+	3.1	No	++
ΔG312-V319	++	6.4	No	+
A322P	++	3.1	No	++
D337H	+	nm	Yes	++
E459K	++	89.7	No	++

'+', decreased protein level or reduced interaction compared with wild-type hGTPBP3.
'++', unchanged protein level or unaffected interaction compared with wild-type hGTPBP3.
nm, not measured.

shorter than the sequence in the NCBI database (514 aa), which lacks exon 8A with 21 amino acids (Figure 7A). To demonstrate whether hGTPBP3-Iso7 was present in other cell lines, we performed RT-PCR analyses using cDNA from various human cell lines, including HEK293T, HeLa, HepG2, AsPC-1, A549, NCI-H446 and NCI-H661. The results showed that hGTPBP3-Iso7 mRNA readily existed in these cell lines (Supplementary Figure S5B). We subsequently designed a pair of primers (Iso7-qp-F and Iso7-qp-R) in the hGTPBP3-Iso7 exon 1A and exon 2 (Figure 7A) and another pair of primers (Iso5-qp-F and Iso5-qp-R) in the hGTPBP3 isoform 5 exon 8A and 8B (Figure 7A) (Supplementary Table S1) to perform real-time quantitative PCR (qPCR). The data revealed that the relative abundance of hGTPBP3-Iso7 mRNA was approximately 12% that of the hGTPBP3 isoforms 4 and 5 in HEK293T cells (Figure 7B).

To further understand whether its mRNA was translated, we raised an anti-hGTPBP3-Iso7 antibody using the S^{18}EPQFPHLQTPDPGDAV^{34} peptide in the hGTPBP3-Iso7 specific N-terminus as an antigen. We expressed genes encoding hGTPBP3 and hGTPBP3-Iso7 with a C-terminal His_6 tag in *E. coli* (Supplementary Figure S5C). The results showed that the anti-hGTPBP3 antibody could simultaneously recognize both proteins (Supplementary Figure S5D); however, overexpressed hGTPBP3-Iso7 but not hGTPBP3 was readily detected using the anti-hGTPBP3-Iso7 antibody (Supplementary Figure S5E), showing its excellent selectivity. In parallel, overexpressed hGTPBP3-Iso7 with a C-terminal FLAG tag (hGTPBP3-Iso7-FLAG) in HEK293T cells could be recognized by the anti-hGTPBP3-Iso7 antibody (Figure 7C, left panel). Then, using HEK293T WCL, we were able to detect a band at the corresponding position, which was not obtained from the mouse C2C12 cell line (Figure 7C, middle and right panels) (note that mouse *Gtpbp3* does not encode a similar isoform). To further confirm that the observed band in HEK293T WCL was endogenous hGTPBP3-Iso7, its mRNA was knocked down by siRNA-104 (Supplementary Figure S5F) (Supplementary Table S1), which specifically targets the mRNA region encoding the hGTPBP3-Iso7 specific N-terminus (Figure 7A). Western blot analysis showed that the corresponding band disappeared (Figure 7D). In addition, endogenous hGTPBP3-Iso7 was pulled down using an anti-hGTPBP3-Iso7 antibody, and the band was excised for mass spectrometry (MS), which detected six fragments of hGTPBP3 despite the unique N-terminus not being captured (Supplementary Figure S5G).

To further understand the cellular localization of hGTPBP3-Iso7, we performed immunofluorescence (IF) analysis of HEK293T cells expressing either hGTPBP3-FLAG or hGTPBP3-Iso7-FLAG. hGTPBP3-Iso7 was indeed distributed in the cytoplasm but not mitochondria, in contrast to mitochondria-localized hGTPBP3 (Figure 7E). The mitochondria and cytoplasm were then separated, and the results confirmed the distribution of hGTPBP3-Iso7 in the cytoplasm (Figure 7F). By expressing the hGTPBP3-Iso7 gene in the *Sc*Δ*MSS1* strain, we found that although the protein level of hGTPBP3-Iso7 was much higher than that of hGTPBP3 (Figure 7G), it was unable to supplement the loss of MSS1 *in vivo* (Figure 7H), likely due to its cytoplasmic but not mitochondrial localization. We performed Co-IP assays in HEK293T cells to explore whether hGTPBP3-Iso7 could form a dimer by overexpressing FLAG- and Myc-tagged hGTPBP3-Iso7. The results showed that hGTPBP3-Iso7-Myc interacted with hGTPBP3-Iso7-FLAG in Co-IP assays using either anti-FLAG antibody (Figure 7I) or anti-Myc antibody (Figure 7J), indicating that hGTPBP3-Iso7 was a homodimer *in vivo*. Taken together, this evidence suggests that a new cytoplasm-localized hGTPBP3-Iso7 was present *in vivo*, and this isoform is not involved in mitochondrial tRNA modification.

DISCUSSION

In *E. coli*, MnmE exhibits high intrinsic GTPase activity, which is essential for its tRNA modification function (50). However, purified human GST-GTPBP3 precursor hydrolyzes GTP at a 100-fold lower rate than *Ec*MnmE and exhibits very low GTPase activity (37). hGTPBP3 localizes in mitochondria (34), and our data clearly showed that it contains an N-terminal extension similar to MTS, which is cleaved after mitochondrial import. In fact, most mitochondrial proteins need to precisely excise MTS in the mitochondrial matrix (43), which is a prerequisite for an active and functional form, such as aminoacyl-tRNA synthetases (e.g. AARS2 (7) and TARS2 (51)) and tRNA modification enzymes (e.g. OSGEPL) (11). Therefore, we suggest the full-length GST-GTPBP3 precursor is inactive in efficiently hydrolyzing GTP *in vitro* because it is not a mature form. In addition, GST appended at the N-terminus may also inhibit its activity. In the present study, we identified the MTS of the hGTPBP3 precursor and determined its mature form. In addition, we successfully established a system to measure the GTPase kinetic parameters of hGTPBP3 *in vitro*, showing that the GTP hydrolysis rate of hGTPBP3 was 20-fold higher than that of the GST-GTPBP3 precursor. In comparison, the k_{cat} value (1.49±0.06 min^{-1}) of

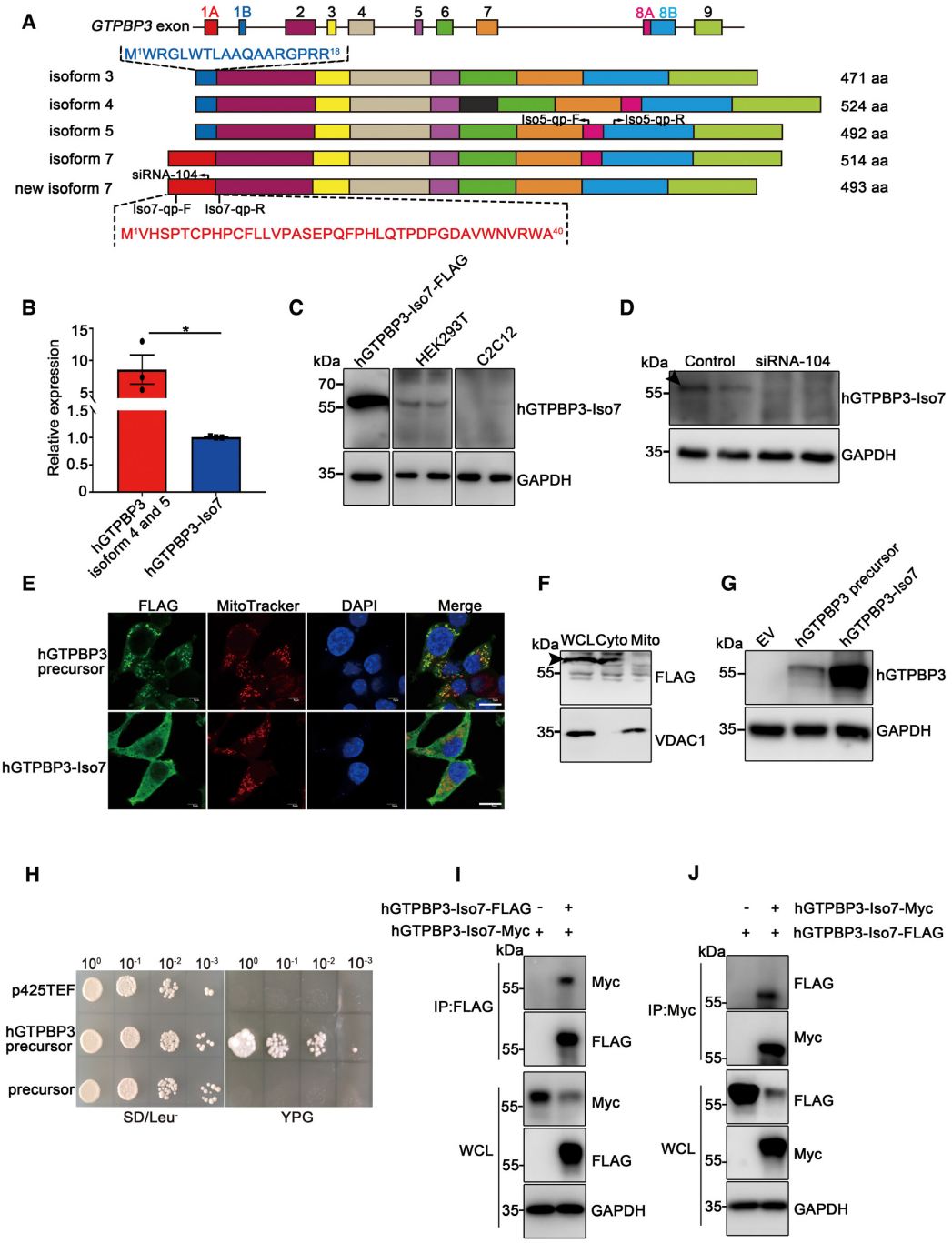

Figure 7. Identification of a new cytoplasm-localized isoform of hGTPBP3. Schematic representation of the hGTPBP3 mRNA structure (**A**) and four NCBI-reported isoforms (lower panel). hGTPBP3 mRNA has nine exons, indicated by different colors. Isoform 4 retained a portion of intron (96 bp, encoding 32 amino acids, indicated by black) between exons 5 and 6. The N-terminal sequences of the hGTPBP3 precursor and hGTPBP3-Iso7 were shown in cyan and red, respectively. The location of siRNA-104 was in exon 1A of hGTPBP3-Iso7. The qPCR primers Iso7-qp-F and Iso7-qp-R were in exon 1A and exon 2 of hGTPBP3-Iso7, respectively. Iso5-qp-F and Iso5-qp-R were in exon 8A and exon 8B, respectively. (**B**) Quantitative PCR analysis showed the relative mRNA level of hGTPBP3-Iso7 (designated 1) compared to that of hGTPBP3 isoform 4 and isoform 5 in HEK293T cells. Error bars: ±SEM; $*P < 0.05$ (Student's *t*-test). (**C**) Detection of endogenous hGTPBP3-Iso7 in HEK293T (middle) or C2C12 (right) cells using an anti-hGTPBP3-Iso7 antibody. Overexpressed hGTPBP3-Iso7-FLAG (left) was used as a positive control. (**D**) The protein level of hGTPBP3-Iso7 treated with siRNA-104 for 72 h was significantly reduced compared with that of the untreated sample. The black arrow indicated endogenous hGTPBP3-Iso7. (**E**) Cellular localization of overexpressed hGTPBP3 precursor or hGTPBP3-Iso7 in HEK293T cells. Images of the hGTPBP3 precursor or hGTPBP3-iso7 (green) and mitochondria (red) and nuclei (blue) were obtained by confocal microscopy. Scale bar: 10 μm. (**F**) Protein level of overexpressed hGTPBP3-Iso7-FLAG in cytoplasm (Cyto) and mitochondria (Mito) in HEK293T cells. The black arrow indicated overexpressed hGTPBP3-Iso7-FLAG. (**G**) Protein levels of the hGTPBP3 precursor and hGTPBP3-Iso7 in the WCL of yeast transformants. (**H**) Yeast complementation of hGTPBP3-Iso7 using the *Sc*Δ*MSS1* strain in the YPG plate. p425TEF or the hGTPBP3 precursor was introduced as a negative or positive control, respectively. (I, J) Genes encoding hGTPBP3-Iso7-Myc and hGTPBP3-Iso7-FLAG were coexpressed in HEK293T cells. hGTPBP3-Iso7-Myc was coprecipitated with hGTPBP3-Iso7-FLAG in Co-IP assays using anti-FLAG antibody (**I**) or anti-Myc antibody (**J**).

hGTPBP3 was 7-fold lower than that of *Ec*MnmE (10.2 min^{-1}) (50), and its K_m value (9.5±1.5 μM) was 54-fold higher than that of *Ec*MnmE (511±53 μM). Therefore, the catalytic efficiency (k_{cat}/K_m) of hGTPBP3 (156.84 min^{-1} mM^{-1}) was 8-fold higher than that of *Ec*MnmE (20 min^{-1} mM^{-1}). Considering the sharp difference in K_m values between the two enzymes, we checked their GTP binding sites. The residues for binding GTP were completely conserved in hGTPBP3, including N259, A260, G261, S263, S264, N374, D377 and S397. It was unclear which elements determined the distinct GTP binding affinities. Mitochondrial proteins are frequently found to be less active than their bacterial homologs. For example, using the same *E. coli* $tRNA^{Leu}$ as a substrate, the catalytic efficiency of human mitochondrial leucyl-tRNA synthetase (hmtLeuRS) (52) was 176-fold lower than that of *E. coli* LeuRS (53). In a parallel report, the catalytic efficiency of hmtLeuRS for mitochondrial $tRNA^{Leu}$(UUR) was reported to be 1500-fold lower than that of *E. coli* LeuRS for *E. coli* $tRNA^{Leu}$(CUN) (54). Our data clearly showed that hGTPBP3 is indeed an active GTPase and exhibits a higher catalytic efficiency than *Ec*MnmE. It has been shown that the *Ec*MnmE G domain exhibits high GTPase activity similar to that of the full-length protein, which needs potassium-dependent dimerization to stimulate GTP hydrolysis (33). We found that the hGTPBP3 G domain and ΔN-hGTPBP3 exhibited very low GTPase activity because of their very high K_m values. Furthermore, potassium and low concentration GDP-AlF_x were unable to induce hGTPBP3 G domain dimerization, in contrast to the *Ec*MnmE G domain, under the same conditions. However, hGTPBP3 G domain and ΔN-hGTPBP3 formed dimers under high GDP-AlF_x concentration.

hGTPBP3 has been identified as a tRNA-modifying enzyme, and its GTPase activity is fundamental for τm^5U modification; however, the biochemical properties of hGTPBP3 have never been characterized. Previous studies have revealed that *Ec*MnmE G domain dimerization and GTP hydrolysis are required for orchestration of the tRNA modification reaction (55). Moreover, *Ec*MnmE interacts with *Ec*MnmG, forming a dynamic complex ($\alpha_2\beta_2$) when GTP is bound (17,46). Our data clearly showed that hGTPBP3 exists as a dimer *in vitro* and *in vivo*, consistent with the *Ec*MnmE conformation. Additionally, we confirmed that hGTPBP3 interacts with hMTO1. Our data clearly showed that GTP hydrolysis by hGTPBP3 is necessary for modification *in vivo*, as evidenced by the fact that two inactive mutants, hGTPBP3-N259A and hGTPBP3-E315A, were unable to support yeast growth *in vivo* under respiratory conditions. Purification of active hGTPBP3 at high purity laid a solid foundation for efficient reconstitution of τm^5U modification *in vitro*. However, the interaction pattern between hGTPBP3 and hMTO1, the mechanism by which the hGTPBP3-hMTO1 complex distinguishes tRNA substrates, and the precise modification mechanism still need to be further explored.

Genetic studies have revealed that mutations in hGTPBP3 lead to mitochondrial dysfunction and human diseases (28). However, the underlying molecular mechanism has not yet been elucidated. In this work, using biochemical, genetic and cell biological methodologies, we systematically elucidated the putative molecular defects of these mutations *in vitro* and *in vivo*. The steady-state protein levels of hGTPBP3-R3L, hGTPBP3-E142K, hGTPBP3-E159V, hGTPBP3-P257H and hGTPBP3-D337H markedly decreased in both WCL and mitochondria, suggesting that these residue sites are important for protein structure and stability. Indeed, the R3L mutation in the MTS of hGTPBP3 impaired mitochondrial import and subsequently led to protein instability. We proposed that R3 is a crucial determinant of hGTPBP3 localization. Subsequently, assays showed that these mutants were clearly ubiquitylated, indicating that they were degraded through the ubiquitin-proteasome pathway. Furthermore, biochemical data showed that the hGTPBP3-E159V, hGTPBP3-A162P, hGTPBP3-P257H, hGTPBP3-A322P, hGTPBP3-E225K/A322P and hGTPBP3-ΔG312-V319 mutants obviously impaired GTPase activity *in vitro*, in line with the fact that they were unable to supplement loss of *Sc*MSS1 *in vivo*, again highlighting the crucial role of GTP hydrolysis in modification *in vivo*. Based on the structure of *Tm*MnmE (PDB: 1XZP), we identified two intradomain interactions, namely, E142-R136 and E159-R431. *In vitro* GTP hydrolysis and *in vivo* complementation assays clearly showed that these two interactions were crucial for maintaining proper structure and function, as evidenced by the restored phenotypes observed upon expression in both yeast and human cells, GTPase activity *in vitro*, steady-state protein level in both WCL and mitochondria and modification activity *in vivo*. Four conserved motifs (G1, G2, G3 and G4) are involved in the binding of guanine nucleotides and Mg^{2+}, regulating the functional state of GTPase (37,50). P257 is located in the G1 motif, and mutation at this key structural site was predicted to disturb binding with GTP and/or disrupt conformational changes in the G domain. Indeed, *in vitro* GTPase kinetics analysis revealed that the K_m value of hGTPBP3-P257H showed the greatest increase among the values for all the mutants. Interestingly, although the hGTPBP3-D337H mutant was unstable in *E. coli* and human cells, it could rescue growth deficiency in yeasts, suggesting that the hGTPBP3-D337H mutant likely had the ability to perform GTP hydrolysis and catalyze tRNA modification *in vivo* if stably expressed. Specifically, hGTPBP3-E459K with full GTPase activity failed to complement the loss of MSS1, and the interaction with hMTO1 was unaffected. We propose that the E459K mutation may influence other processes in tRNA modification, such as tRNA or cofactor binding. Collectively, our data allow direct elucidation of the potential molecular mechanism of the pathogenic mutations of hGTPBP3.

Five splicing variants of hGTPBP3 have been reported (34), but only four isoforms could be translated to proteins, among which isoform 5 was firmly established (37). Herein, we experimentally confirmed a novel hGTPBP3 isoform named hGTPBP3-Iso7 in human cells; this isoform harbors a unique N-terminus, different from those of other isoforms. Our results clearly showed that hGTPBP3-Iso7 mRNA was indeed translated to protein and could be detected by an antibody, although the mRNA abundance was much lower than that of other hGTPBP3 precursors, suggesting that hGTPBP3-Iso7 was stable *in vivo*. Interestingly, hGTPBP3-Iso7 localizes in the cytoplasm but not mitochondria due to its distinct N-terminus. As expected,

hGTPBP3-Iso7 failed to rescue yeast growth, likely because it could not be imported into mitochondria. These findings hint that hGTPBP3-Iso7 has unidentified novel functions, possibly performing GTP hydrolysis in cellular pathways other than tRNA modification. The physiological role of hGTPBP3-Iso7 needs to be further explored.

SUPPLEMENTARY DATA

Supplementary Data are available at NAR Online.

ACKNOWLEDGEMENTS

We are grateful to Dr Min-Xin Guan (Zhejiang University) for providing the *Sc*Δ*MSS1* strain. We also thank Dr Rong-gui Hu (Shanghai Institute of Biochemistry and Cell Biology) for providing the plasmid encoding HA-Ub.

FUNDING

National Key Research and Development Program of China [2017YFA0504000]; Natural Science Foundation of China [91440204, 31500644, 31570792, 31670801, 31822015, 81870896, 31870811]; Strategic Priority Research Program of the Chinese Academy of Sciences [XDB19010203]; Shanghai Key Laboratory of Embryo Original Diseases [Shelab201904]. Funding for open acecss charge: Natural Science Foundation of China [81870896, 31670801].
Conflict of interest statement. None declared.

REFERENCES

1. Chan,D.C. (2006) Mitochondria: dynamic organelles in disease, aging, and development. *Cell*, **125**, 1241–1252.
2. Wallace,D.C. (2005) A mitochondrial paradigm of metabolic and degenerative diseases, aging, and cancer: a dawn for evolutionary medicine. *Annu. Rev. Genet.*, **39**, 359–407.
3. Anderson,S., Bankier,A.T., Barrell,B.G., de Bruijn,M.H., Coulson,A.R., Drouin,J., Eperon,I.C., Nierlich,D.P., Roe,B.A., Sanger,F. *et al.* (1981) Sequence and organization of the human mitochondrial genome. *Nature*, **290**, 457–465.
4. Suzuki,T., Nagao,A. and Suzuki,T. (2011) Human mitochondrial tRNAs: biogenesis, function, structural aspects, and diseases. *Annu. Rev. Genet.*, **45**, 299–329.
5. Wang,Y., Zeng,Q.Y., Zheng,W.Q., Ji,Q.Q., Zhou,X.L. and Wang,E.D. (2018) A natural non-Watson-Crick base pair in human mitochondrial $tRNA^{Thr}$ causes structural and functional susceptibility to local mutations. *Nucleic Acids Res.*, **46**, 4662–4676.
6. Antonellis,A. and Green,E.D. (2008) The role of aminoacyl-tRNA synthetases in genetic diseases. *Annu. Rev. Genomics Hum. Genet.*, **9**, 87–107.
7. Zeng,Q.Y., Peng,G.X., Li,G., Zhou,J.B., Zheng,W.Q., Xue,M.Q., Wang,E.D. and Zhou,X.L. (2019) The G3-U70-independent tRNA recognition by human mitochondrial alanyl-tRNA synthetase. *Nucleic Acids Res.*, **47**, 3072–3085.
8. Wang,Y., Zhou,J.B., Zeng,Q.Y., Wu,S., Xue,M.Q., Fang,P., Wang,E.D. and Zhou,X.L. (2020) Hearing impairment-associated KARS mutations lead to defects in aminoacylation of both cytoplasmic and mitochondrial $tRNA^{Lys}$. *Sci China Life Sci*, **63**, 1227–1239.
9. Zheng,W.Q., Zhang,Y., Yao,Q., Chen,Y., Qiao,X., Wang,E.D., Chen,C. and Zhou,X.L. (2020) Nitrosative stress inhibits aminoacylation and editing activities of mitochondrial threonyl-tRNA synthetase by S-nitrosation. *Nucleic Acids Res.*, **48**, 6799–6810.
10. de Crécy-Lagard,V., Boccaletto,P., Mangleburg,C.G., Sharma,P., Lowe,T.M., Leidel,S.A. and Bujnicki,J.M. (2019) Matching tRNA modifications in humans to their known and predicted enzymes. *Nucleic Acids Res.*, **47**, 2143–2159.
11. Zhou,J.B., Wang,Y., Zeng,Q.Y., Meng,S.X., Wang,E.D. and Zhou,X.L. (2020) Molecular basis for t^6A modification in human mitochondria. *Nucleic Acids Res.*, **48**, 3181–3194.
12. Suzuki,T. and Suzuki,T. (2014) A complete landscape of post-transcriptional modifications in mammalian mitochondrial tRNAs. *Nucleic Acids Res.*, **42**, 7346–7357.
13. Suzuki,T., Yashiro,Y., Kikuchi,I., Ishigami,Y., Saito,H., Matsuzawa,I., Okada,S., Mito,M., Iwasaki,S., Ma,D. *et al.* (2020) Complete chemical structures of human mitochondrial tRNAs. *Nat. Commun.*, **11**, 4269.
14. Motorin,Y. and Helm,M. (2010) tRNA stabilization by modified nucleotides. *Biochemistry*, **49**, 4934–4944.
15. Nedialkova,D.D. and Leidel,S.A. (2015) Optimization of codon translation rates via tRNA modifications maintains proteome integrity. *Cell*, **161**, 1606–1618.
16. Moukadiri,I., Prado,S., Piera,J., Velazquez-Campoy,A., Bjork,G.R. and Armengod,M.E. (2009) Evolutionarily conserved proteins MnmE and GidA catalyze the formation of two methyluridine derivatives at tRNA wobble positions. *Nucleic Acids Res.*, **37**, 7177–7193.
17. Yim,L., Moukadiri,I., Bjork,G.R. and Armengod,M.E. (2006) Further insights into the tRNA modification process controlled by proteins MnmE and GidA of *Escherichia coli*. *Nucleic Acids Res.*, **34**, 5892–5905.
18. Wang,X., Yan,Q. and Guan,M.X. (2010) Combination of the loss of $cmnm^5U_{34}$ with the lack of s^2U_{34} modifications of $tRNA^{Lys}$, $tRNA^{Glu}$, and $tRNA^{Gln}$ altered mitochondrial biogenesis and respiration. *J. Mol. Biol.*, **395**, 1038–1048.
19. Asano,K., Suzuki,T., Saito,A., Wei,F.Y., Ikeuchi,Y., Numata,T., Tanaka,R., Yamane,Y., Yamamoto,T., Goto,T. *et al.* (2018) Metabolic and chemical regulation of tRNA modification associated with taurine deficiency and human disease. *Nucleic Acids Res.*, **46**, 1565–1583.
20. Sasarman,F., Antonicka,H., Horvath,R. and Shoubridge,E.A. (2011) The 2-thiouridylase function of the human MTU1 (TRMU) enzyme is dispensable for mitochondrial translation. *Hum. Mol. Genet.*, **20**, 4634–4643.
21. Kirino,Y., Yasukawa,T., Ohta,S., Akira,S., Ishihara,K., Watanabe,K. and Suzuki,T. (2004) Codon-specific translational defect caused by a wobble modification deficiency in mutant tRNA from a human mitochondrial disease. *Proc. Natl. Acad. Sci. U.S.A.*, **101**, 15070–15075.
22. Kurata,S., Weixlbaumer,A., Ohtsuki,T., Shimazaki,T., Wada,T., Kirino,Y., Takai,K., Watanabe,K., Ramakrishnan,V. and Suzuki,T. (2008) Modified uridines with C5-methylene substituents at the first position of the tRNA anticodon stabilize U.G wobble pairing during decoding. *J. Biol. Chem.*, **283**, 18801–18811.
23. Yasukawa,T., Suzuki,T., Ishii,N., Ueda,T., Ohta,S. and Watanabe,K. (2000) Defect in modification at the anticodon wobble nucleotide of mitochondrial $tRNA^{Lys}$ with the MERRF encephalomyopathy pathogenic mutation. *FEBS Lett.*, **467**, 175–178.
24. Tischner,C., Hofer,A., Wulff,V., Stepek,J., Dumitru,I., Becker,L., Haack,T., Kremer,L., Datta,A.N., Sperl,W. *et al.* (2015) MTO1 mediates tissue specificity of OXPHOS defects via tRNA modification and translation optimization, which can be bypassed by dietary intervention. *Hum. Mol. Genet.*, **24**, 2247–2266.
25. Suzuki,T., Suzuki,T., Wada,T., Saigo,K. and Watanabe,K. (2002) Taurine as a constituent of mitochondrial tRNAs: new insights into the functions of taurine and human mitochondrial diseases. *EMBO J.*, **21**, 6581–6589.
26. Shoffner,J.M., Lott,M.T., Lezza,A.M., Seibel,P., Ballinger,S.W. and Wallace,D.C. (1990) Myoclonic epilepsy and ragged-red fiber disease (MERRF) is associated with a mitochondrial DNA $tRNA^{Lys}$ mutation. *Cell*, **61**, 931–937.
27. Goto,Y., Nonaka,I. and Horai,S. (1990) A mutation in the $tRNA^{Leu(UUR)}$ gene associated with the MELAS subgroup of mitochondrial encephalomyopathies. *Nature*, **348**, 651–653.
28. Kopajtich,R., Nicholls,T.J., Rorbach,J., Metodiev,M.D., Freisinger,P., Mandel,H., Vanlander,A., Ghezzi,D., Carrozzo,R., Taylor,R.W. *et al.* (2014) Mutations in GTPBP3 cause a

mitochondrial translation defect associated with hypertrophic cardiomyopathy, lactic acidosis, and encephalopathy. *Am. J. Hum. Genet.*, **95**, 708–720.
29. Fakruddin,M., Wei,F.Y., Suzuki,T., Asano,K., Kaieda,T., Omori,A., Izumi,R., Fujimura,A., Kaitsuka,T., Miyata,K. *et al.* (2018) Defective mitochondrial tRNA taurine modification activates global proteostress and leads to mitochondrial disease. *Cell Rep.*, **22**, 482–496.
30. Charif,M., Titah,S.M., Roubertie,A., Desquiret-Dumas,V., Gueguen,N., Meunier,I., Leid,J., Massal,F., Zanlonghi,X., Mercier,J. *et al.* (2015) Optic neuropathy, cardiomyopathy, cognitive disability in patients with a homozygous mutation in the nuclear MTO1 and a mitochondrial MT-TF variant. *Am. J. Med. Genet. A*, **167a**, 2366–2374.
31. Ghezzi,D., Baruffini,E., Haack,T.B., Invernizzi,F., Melchionda,L., Dallabona,C., Strom,T.M., Parini,R., Burlina,A.B., Meitinger,T. *et al.* (2012) Mutations of the mitochondrial-tRNA modifier MTO1 cause hypertrophic cardiomyopathy and lactic acidosis. *Am. J. Hum. Genet.*, **90**, 1079–1087.
32. Chen,D., Zhang,Z., Chen,C., Yao,S., Yang,Q., Li,F., He,X., Ai,C., Wang,M. and Guan,M.X. (2019) Deletion of Gtpbp3 in zebrafish revealed the hypertrophic cardiomyopathy manifested by aberrant mitochondrial tRNA metabolism. *Nucleic Acids Res.*, **47**, 5341–5355.
33. Scrima,A. and Wittinghofer,A. (2006) Dimerisation-dependent GTPase reaction of MnmE: how potassium acts as GTPase-activating element. *EMBO J.*, **25**, 2940–2951.
34. Li,X. and Guan,M.X. (2002) A human mitochondrial GTP binding protein related to tRNA modification may modulate phenotypic expression of the deafness-associated mitochondrial 12S rRNA mutation. *Mol. Cell. Biol.*, **22**, 7701–7711.
35. Scrima,A., Vetter,I.R., Armengod,M.E. and Wittinghofer,A. (2005) The structure of the TrmE GTP-binding protein and its implications for tRNA modification. *EMBO J.*, **24**, 23–33.
36. Cabedo,H., Macián,F., Villarroya,M., Escudero,J., Martinez-Vicente,M., Knecht,E. and Armengod,M. (1999) The *Escherichia coli* trmE (mnmE) gene, involved in tRNA modification, codes for an evolutionarily conserved GTPase with unusual biochemical properties. *EMBO J.*, **18**, 7063–7076.
37. Villarroya,M., Prado,S., Esteve,J.M., Soriano,M.A., Aguado,C., Pérez-Martínez,D., Martínez-Ferrandis,J.I., Yim,L., Victor,V.M., Cebolla,E. *et al.* (2008) Characterization of human GTPBP3, a GTP-binding protein involved in mitochondrial tRNA modification. *Mol. Cell. Biol.*, **28**, 7514–7531.
38. Ye,Q., Ji,Q.Q., Yan,W., Yang,F. and Wang,E.D. (2017) Acetylation of lysine ϵ-amino groups regulates aminoacyl-tRNA synthetase activity in Escherichia coli. *J. Biol. Chem.*, **292**, 10709–10722.
39. Wieckowski,M.R., Giorgi,C., Lebiedzinska,M., Duszynski,J. and Pinton,P. (2009) Isolation of mitochondria-associated membranes and mitochondria from animal tissues and cells. *Nat. Protoc.*, **4**, 1582–1590.
40. Mumberg,D., Müller,R. and Funk,M. (1995) Yeast vectors for the controlled expression of heterologous proteins in different genetic backgrounds. *Gene*, **156**, 119–122.
41. Zhou,X.L., Chen,Y., Fang,Z.P., Ruan,Z.R., Wang,Y., Liu,R.J., Xue,M.Q. and Wang,E.D. (2016) Translational quality control by bacterial threonyl-tRNA synthetases. *J. Biol. Chem.*, **291**, 21208–21221.
42. Yuan,J.S., Reed,A., Chen,F. and Stewart,C.N. Jr (2006) Statistical analysis of real-time PCR data. *BMC Bioinformatics*, **7**, 85.
43. Neupert,W. and Herrmann,J.M. (2007) Translocation of proteins into mitochondria. *Annu. Rev. Biochem.*, **76**, 723–749.
44. Carapito,C., Kuhn,L., Karim,L., Rompais,M., Rabilloud,T., Schwenzer,H. and Sissler,M. (2017) Two proteomic methodologies for defining N-termini of mature human mitochondrial aminoacyl-tRNA synthetases. *Methods*, **113**, 111–119.
45. Colby,G., Wu,M. and Tzagoloff,A. (1998) MTO1 codes for a mitochondrial protein required for respiration in paromomycin-resistant mutants of Saccharomyces cerevisiae. *J. Biol. Chem.*, **273**, 27945–27952.
46. Fislage,M., Brosens,E., Deyaert,E., Spilotros,A., Pardon,E., Loris,R., Steyaert,J., Garcia-Pino,A. and Versées,W. (2014) SAXS analysis of the tRNA-modifying enzyme complex MnmE/MnmG reveals a novel interaction mode and GTP-induced oligomerization. *Nucleic Acids Res.*, **42**, 5978–5992.
47. Han,Y.H., Moon,H.J., You,B.R. and Park,W.H. (2009) The effect of MG132, a proteasome inhibitor on HeLa cells in relation to cell growth, reactive oxygen species and GSH. *Oncol. Rep.*, **22**, 215–221.
48. Haspel,J., Shaik,R.S., Ifedigbo,E., Nakahira,K., Dolinay,T., Englert,J.A. and Choi,A.M. (2011) Characterization of macroautophagic flux in vivo using a leupeptin-based assay. *Autophagy*, **7**, 629–642.
49. Zhou,X.L., Ruan,Z.R., Wang,M., Fang,Z.P., Wang,Y., Chen,Y., Liu,R.J., Eriani,G. and Wang,E.D. (2014) A minimalist mitochondrial threonyl-tRNA synthetase exhibits tRNA-isoacceptor specificity during proofreading. *Nucleic Acids Res.*, **42**, 13873–13886.
50. Yim,L., Martinez-Vicente,M., Villarroya,M., Aguado,C., Knecht,E. and Armengod,M.-E. (2003) The GTPase activity and C-terminal cysteine of the *Escherichia coli* MnmE protein are essential for its tRNA modifying function. *J. Biol. Chem.*, **278**, 28378–28387.
51. Wang,Y., Zhou,X.L., Ruan,Z.R., Liu,R.J., Eriani,G. and Wang,E.D. (2016) A human disease-causing point mutation in mitochondrial threonyl-tRNA synthetase Induces both structural and functional defects. *J. Biol. Chem.*, **291**, 6507–6520.
52. Yao,Y.N., Wang,L., Wu,X.F. and Wang,E.D. (2003) Human mitochondrial leucyl-tRNA synthetase with high activity produced from Escherichia coli. *Protein Expr. Purif.*, **30**, 112–116.
53. Li,T., Li,Y., Guo,N., Wang,E. and Wang,Y. (1999) Discrimination of $tRNA^{Leu}$ isoacceptors by the insertion mutant of *Escherichia coli* leucyl-tRNA synthetase. *Biochemistry*, **38**, 9084–9088.
54. Lue,S.W. and Kelley,S.O. (2007) A single residue in leucyl-tRNA synthetase affecting amino acid specificity and tRNA aminoacylation. *Biochemistry*, **46**, 4466–4472.
55. Meyer,S., Wittinghofer,A. and Versees,W. (2009) G-domain dimerization orchestrates the tRNA wobble modification reaction in the MnmE/GidA complex. *J. Mol. Biol.*, **392**, 910–922.